Agricultural Water Management 298 (2024) 108861

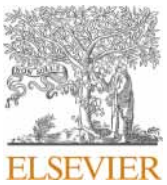

Contents lists available at ScienceDirect

Agricultural Water Management

journal homepage: www.elsevier.com/locate/agwat

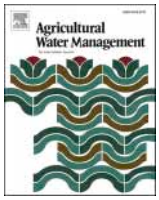

Assessment of the modified two-source energy balance (TSEB) model for estimating evapotranspiration and its components over an irrigated olive orchard in Morocco

Ourrai Sara [a,*], Aithssaine Bouchra [b], Amazirh Abdelhakim [b], Er-RAKI Salah [b,c], Bouchaou Lhoussaine [a,d], Jacob Frederic [e], Chehbouni Abdelghani [a,b]

[a] Mohammed VI Polytechnic University, International Water Research Institute (IWRI), Benguerir, Morocco
[b] Mohammed VI Polytechnic University, Center for Remote Sensing Applications (CRSA), Benguerir, Morocco
[c] Cadi Ayyad University, Department of Applied Physics, Faculty of Sciences and technologies, ProcEDE/AgroBiotech center, Marrakech, Morocco
[d] Ibn Zohr University, Laboratory of Applied Geology and Geo Environment (LAGAGE), Faculty of Sciences, Agadir, Morocco
[e] LISAH, University of Montpellier, AgroParisTech, INRAE, Institut Agro Montpellier, IRD, Montpellier, France

ARTICLE INFO

Handling Editor- J.E. Fernández

Keywords:
Evapotranspiration
Priestley-Taylor coefficient
Trees
ET partitioning
Arid zones

ABSTRACT

Olives constitute a frequently grown crop in semi-arid areas. Therefore, accurate quantification of evapotranspiration (ET) within olive groves is crucial to enhance agricultural water productivity and promote their resilience to water scarcity and future climate scenarios. In the present work, we assessed the accuracy of 3 versions of the Two-Source-Energy-Balance (TSEB) model, the first one "TSEB-SPT" using a standard Priestley-Taylor coefficient (αPT) to estimate the transpiration, the second one called "TSEB-CPT" constrained by a computed αPT using measured ET along with the equilibrium term, and the third one "TSEB-SM" where soil moisture is used as an additional constraint to improve the soil evaporation. The 3 models were applied over an irrigated olive orchard in the Tensift basin (Morocco) during two growing periods of 2003 and 2004. The comparison with ground-based flux measurements from Eddy-Covariance tower and sap flow data revealed that the TSEB-SPT model overestimates ET with an average relative error of 87% and a percentage bias of -78% during the two growing seasons. Conversely, TSEB-SM and TSEB-CPT improved ET estimates as compared to TSEB-SPT, with mean relative errors of 31% and 24% and an average percentage bias of 0.6% and -7.4%, respectively. For ET partitioning, TSEB-SM appears to be less effective in estimating transpiration, while the simulated transpiration by TSEB-CPT fits well the actual one with a root mean square error of 0.27 mm, mainly during the summer of 2003. These results open a path for future improvements: by reviewing the calibration procedure of αPT, and implementing alternative formulas to compute the evaporation, the TSEB-SM could be potentially a robust tool for monitoring the seasonal variation of ET and its partitioning over a heterogeneous canopy cover.

1. Introduction

Over the last 100 years, global water consumption has risen sixfold and is still growing gradually at a pace of roughly 1% per year due to expanding populations, economic development, and evolving consumption patterns (WWAP, 2020). Climate change will exacerbate the situation in regions that already experience water stress, and will cause water stress in some areas where there are presently plentiful water resources. Agriculture is considered the primary user of water resources, accounting for 69% of global freshwater withdrawals (AQUASTAT, 2014; WWAP, 2020). As a result, managing agricultural water is essential to adjust the supply-demand balance, regulate the demand, and help decision-makers to effectively allocate available water to various uses (Bashir et al., 2008).

Specific concerns for agricultural water management under climate change are twofold. The first challenge is adjusting current production modes to deal with increased occurrences of water scarcity, and the second one is to implement climate mitigation strategies that lower greenhouse gas emissions and improve water availability in order to respond to policy initiatives to "decarbonize" agriculture (WWAP, 2020). A variety of adaptative strategies have been supported to sustain current levels of agricultural production and increase the efficiency of

* Corresponding author.
E-mail address: sara.ourrai@um6p.ma (O. Sara).

https://doi.org/10.1016/j.agwat.2024.108861
Received 30 November 2023; Received in revised form 31 March 2024; Accepted 5 May 2024
Available online 13 May 2024
0378-3774/© 2024 The Author(s). Published by Elsevier B.V. This is an open access article under the CC BY-NC license (http://creativecommons.org/licenses/by-nc/4.0/).

water use. Precision irrigation is widely employed and is commonly defined as precise water delivery to crop at the right time, at the right place, with the right amount and the right manner (Abioye et al., 2020; Fernández et al., 2018; Khriji et al., 2014). In fact, a precise estimate of crop water requirements, also known as crop evapotranspiration (ETc), can be used to quantify the appropriate amount of irrigation, thereby helping to better manage irrigation and increase water use efficiency throughout the growing season (Ait Hssaine et al., 2021; Allen et al., 2011; Amazirh et al., 2017; Elfarkh et al., 2022 ; Er-Raki et al., 2007; Kharrou et al., 2013; Pereira et al., 2015; Rozenstein et al., 2023; Yimam et al., 2015).

Olive trees constitute one of the Mediterranean region's major strategic crops, due to their high adaptability to dry spells and their ability to achieve acceptable yields under dry conditions (Ezzahar et al., 2007; Fernández et al., 1997; Kassout et al., 2021; Tanasijevic et al., 2014; Wahbi et al., 2005). They cover around 10.5 million hectares, accounting for 98% of the world's olive cultivated areas (FAOSTAT,2023). In Morocco, olive growing dominates the arboreal sector, covering 1.1 million hectares and producing 1.6 billion kilograms in 2021, according to FAOSTAT (FAOSTAT, 2023). Furthermore, it generates 5% of the agricultural gross domestic product and thus plays an essential role in supporting economy and jobs (Bouhafa, 2022). Then, climate-smart management is required for olive crops in order to promote their resilience to future climate scenarios (Aguirre-García et al., 2021). Accordingly, an accurate estimation of ETc of olive groves is crucial for optimizing water management and maximizing crop productivity.

Over recent years, various models have been designed to simulate actual evapotranspiration (ET) with several levels of accuracy (Acharya and Sharma, 2021; Ait Hssaine et al., 2018; Amazirh et al., 2017; Colaizzi et al., 2014; Diarra et al., 2017; Elfarkh et al., 2022 ; Gan et al., 2019; Kato et al., 2004; Merlin et al., 2014; Saadi et al., 2018; Toumi et al., 2016; Zhang et al., 2008). Surface-Energy-Balance (SEB) models are among the most widely used and physically-based concept for capturing and characterizing land surface processes. SEB models rely on the solving of surface energy budget and are driven by Land Surface Temperature (LST) as a significant constraint. According to Kalma et al. (2008), LST-based SEB models are categorized as: one-source models, which treat soil and vegetation as a unique element of the energy-budget, two-source models, which account for the individual contributions of soil and vegetation to the total heat flux, as well as multi-layer models, which are merely extensions of the two-source models (Bastiaanssen. et al., 1998; Kalma et al., 2008; Norman et al., 1995; Su, 2002; Yang et al., 2015).

The Two-Source-Energy-Balance (TSEB) model developed by Norman et al. (1995) and Kustas and Norman (1999) is one of the several existing dual-source ET models. Its ability to estimate latent heat flux for various canopy covers has been reported in numerous studies (Aguirre-García et al., 2021; Ait Hssaine et al., 2018; Bellvert et al., 2020; Elfarkh et al., 2020; Gao et al., 2023; Gómez-Candón et al., 2021; Nieto et al., 2022). The TSEB model computes fluxes and splits available energy between soil and vegetation components using two main inputs as critical boundary conditions, namely LST and leaf area index (LAI). The canopy transpiration (T) is estimated in the TSEB scheme using the Priestley-Taylor (PT) approach, and the Priestley-Taylor coefficient (αPT) is set to its 1.26 standard value and reduced iteratively to take water-limited conditions into account. Shortly, when negative soil evaporation (E) results, which is not a realistic solution during the daytime conditions, the αPT value is lowered and the fluxes and temperatures are recalculated in an iterative process until a positive soil latent heat flux value is reached (Anderson, 2012). Nevertheless, the increase in αPT under extremely advective conditions or high diurnal variation of vapor pressure deficit (VPD), which is a typical characteristic of arid and semi-arid climates, is not taken into consideration and might cause T to be underestimated (Song et al., 2016). This issue could be overcome if the Penman-Monteith (PM) approach is adopted instead of the PT formulation in the TSEB model (Colaizzi et al., 2014). However, the PM approach needs several input data, which are usually not available at large scales. Then, finding the suitable value for the αPT coefficient is critical to successfully implement the PT approach. Several studies have shown that the estimates of latent heat flux (LE) could be improved. First possibility consists of computing αPT on the basis of ET partitioning and plant physiological limitations, where the latter is defined as a function of readily available characteristics such as LAI and air temperature (Ai and Yang, 2016). Second possibility consists of using LE measurements and the equilibrium term (radiative term of PM formula), which is defined by Slatyer and McIlroy (1961) as the limit reached over a long fetch when unsaturated air comes into contact with a moist surface; thus the αPT is derived from the ratio of LE measurements to the equilibrium term (Wu et al., 2021). Third possibility consists of expressing αPT as a calibrated empirical function of VPD (Agam et al., 2010; Tanner and Jury, 1976).

Under water-scarce conditions, LST may not constrain E and T concurrently. Accordingly, the soil moisture (SM) information has been integrated into the TSEB model, as an additional constraint in conjunction with LST, in order to enhance ET estimates over semi-arid regions (Ait Hssaine et al., 2018; Song et al., 2016). Indeed, Ait Hssaine et al. (2021) demonstrated that the TSEB-SM model considerably enhanced ET estimates over irrigated wheat fields in a semi-arid region, through (1) the adjustment of the αPT coefficient to account for soil water content, and (2) a calibration approach to provide soil texture-dependent coefficients using near-surface SM to determine E. Also, Song et al. (2022) suggested a revised version of the TSEB by coupling SM with E and T algorithms to accurately estimate ET and its components over different land covers (grassland, shrub-forest, irrigated cropland and desert steppe) with various SM levels ranging from completely wet to extremely dry SM conditions.

In the context of olive orchard management, the accurate quantification of ET is essential for optimizing water use and ensuring sustainable agricultural practices. Several studies have advanced our understanding of ET estimation (Cammalleri et al., 2013a, 2010; Er-Raki et al., 2008; Fuentes-Peñailillo et al., 2018; Hoedjes et al., 2008; Ortega-Farías, S. and López-Olivari, 2012; Ortega-Farías et al., 2016), and the partitioning of ET components by coupling sap flow data to Eddy-Covariance (EC) measurements (Cammalleri et al., 2013b; López-Olivari et al., 2016), or using the FAO-56 dual crop coefficient model (Er-Raki et al., 2010). The energy balance models used in these previous studies, namely TSEB and Shuttleworth-Wallace (Shuttleworth and Wallace, 1985), relied on limited boundary conditions to estimate ET and its components over olive orchards, typically employing LST and LAI (or vegetation cover) or SM and Normalized Difference Vegetation Index (NDVI). Despite these advancements, the application of a model that integrates three boundary conditions (LST, LAI and SM), to simultaneously estimate ET and its components over a flood-irrigated olive orchard under semi-arid conditions remains unexplored. Our work addresses this gap by implementing a novel modeling approach, and examines the impact of the calibration procedure of the αPT coefficient, along with the introduction of near-surface SM on the estimation of ET over arboreal systems, particularly olive orchards.

The primary aim of this work is to assess the performance of three versions of TSEB model in simulating ET and estimating its components, which are vital for understanding tree functioning and agricultural productivity, especially for olive orchard. Specifically, we aim to: (1) Compare simulated fluxes from the original TSEB run with the standard value of αPT coefficient (TSEB-SPT), with a computed one (TSEB-CPT), and TSEB-SM (coupled to soil moisture) against flux measurements from the EC system; and (2) Assess the accuracy of these models in estimating ET components by integrating EC measurements with scaled sap flow data, highlighting their capability to capture transpiration dynamics, a key factor in regional ET that is directly related to tree functioning and olive production.

2. Materials and methods

2.1. Study site

The experiment was carried out within the Agdal olive orchard, located south-east of Marrakech city, Morocco (Fig. 1). This area is characterized by a semi-arid Mediterranean climate, with an average annual precipitation of 240 mm, and reference evapotranspiration (computed according to the FAO-56 procedure (Allen et al., 1998)) of about 1500 mm (Diarra et al., 2017; Duchemin et al., 2006; Er-Raki et al., 2010).

The research field consisted of 240 year old olive trees, cultivated in an orchard of around 275 ha, with a planting density of 225 trees/ha (Williams et al., 2004). The olive trees were roughly 6 m height on average. Natural grass covered partially the soil surface (15–20%). This percentage was stated by (Er-Raki et al., 2010, 2008; Hoedjes et al., 2007). The orchard was surface irrigated using flood irrigation for a total of eight times, with roughly 100 mm of water supplies per irrigation event (see Fig. 3) (Er-Raki et al., 2010, 2008; Williams et al., 2004).

2.2. Description of site data

2.2.1. Eddy-Covariance (EC) measurements and meteorological data

We provide here an overview about the EC and meteorological data. Further information on the location and type of instruments used to collect data over the study site can be found in Er-Raki et al. (2008).

A standard micrometeorological weather station was used to collect classical climatic data over olive trees (wind speed, rainfall, incoming solar radiation, air temperature and humidity). Soil moisture was measured every thirty minutes at multiple depths (5, 10, 20, 30, 40 cm) using Time Domain Reflectometry (TDR) probes (CS616, Campbell Scientific Ltd).

A CNR1 net radiometer by Kipp & Zonen was used to measure the incoming and outgoing shortwave and longwave. Soil heat flux plates (Hukseflux) were used to measure soil heat flux (G) at 1 cm depth, and were placed in three locations according to the diurnal course of solar position: one beneath the tree (always shaded), one in the middle, and one between the trees. The semi-hourly average values of G, derived from the flux plates served as input for the three versions of TSEB model. It was noticed that the estimates of LE and H fluxes associated with these inputs resulted in substantial errors. This was expected, because G is often regarded as a difficult component to quantify. In fact, the plates must be completely covered to prevent them from being exposed to sunlight, as well as to precipitation events that might modify plates exposure, so that G measurements are not affected (Ait Hssaine et al., 2021). Therefore, in the present study, a value of 0.5 is assigned to the fraction of soil net radiation (Rns) (calculated using Rn measurements) used to compute G.

The H and LE heat fluxes were measured using an EC system at a 9.2 m height with a 20 Hz sampling frequency. The EC system was made up of a 3D sonic anemometer (CSAT3, Campbell Scientific Ltd.) and an open path infrared gas analyzer (Li7500, Licor Inc.). The source area of the EC tower, computed using the analytical footprint model proposed by Horst and Weil (1994), (1992), was approximately 40 m in the northwestern direction (Er-Raki et al., 2008), where 90% of the flux typically arose from within 40 m of the EC system (Hoedjes et al., 2007). Therefore, the EC tower measurements are presumed to be representative of the field scale.

Data collected during the daytime hours from 09:00–17:00 were utilized throughout the whole growing seasons of 2003 and 2004. The energy balance closure was used to assess the performance of flux measurements. The comparison between the half-hourly available energy and turbulent fluxes measured by the EC system revealed that turbulent fluxes were underestimated by roughly 12% in 2003 and 2% in 2004 (data not displayed here). The energy balance closure was improved by using the Bowen ratio approach (Twine et al., 2000).

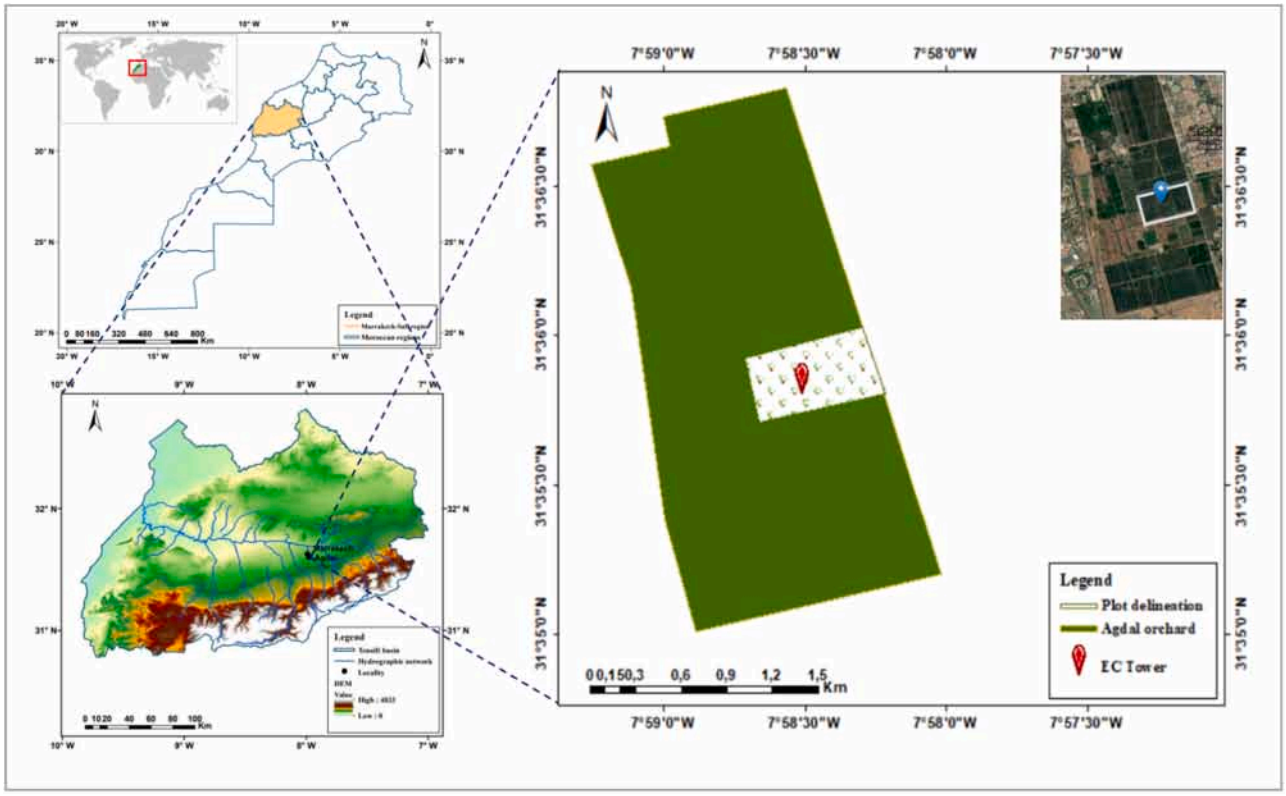

Fig. 1. Overall location of Tensift basin and the study site "Agdal", along with the location of the Eddy-Covariance (EC) tower within the study site.

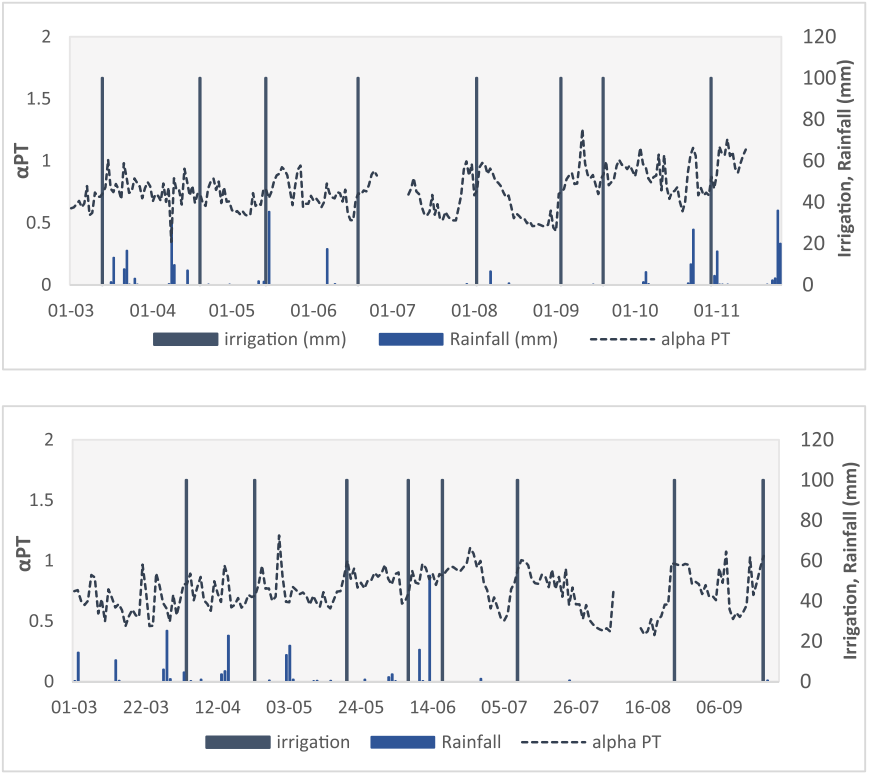

Fig. 3. Seasonal variation of daily αPT coefficient at Agdal site during the growing seasons of 2003 (top) and 2004 (bottom). The amounts of precipitation and irrigation are also plotted as bar charts.

2.2.2. Sap flow data measurements

Sap flow was measured using Heat-Ratio-Method (HRM), which was developed by Burgess et al. (2001) to measure the xylem sap flow. The HRM method is a modification of the Heat- Pulse-Method (HPM) technique, which involves the insertion of temperature probes into the active xylem at similar distances downstream and upstream from a heat source. Williams et al. (2004) provided a detailed overview of the HRM technique and measurement fundamentals.

The HRM technique outperforms the HPM in determining the transpiration (T) accurately at very low flow rates. In addition, its reliability has been demonstrated by other studies (Burgess et al., 2001; Fernaández et al., 2001; Williams et al., 2004). The principal drawback of the sap flow approach is the scaling from the sensor to the tree and from the tree to the stand (Granier, 1987). Thus, combining two or more methods of ET measurements together is the simplest way to overcome the restrictions of each approach when used separately. Er-Raki et al. (2009) demonstrated that combining sap flow and Eddy-covariance methods produced more reliable estimates of E and T. Moreover, Cammalleri et al. (2013b) undertook a comprehensive evaluation to unravel the contributions of actual crop transpiration and soil evaporation to the water dynamics of a Mediterranean olive orchard. They were able to accurately determine the respective contributions of these processes to overall evapotranspiration by leveraging the joint application of eddy covariance and sap flow measurements, resulting in a precise understanding of the balance between soil moisture loss and plant water consumption.

The sap flow sensors were setup on eight olive trees within the source area of the EC tower, including four large multi-stemmed and four single-stemmed trees. Sap flow measurements were carried out during the summer periods, from 12 June to 30 July in 2003, and from 9 May to 28 September in 2004.

2.2.3. Remote sensing data

To conduct our analysis with the three versions of TSEB model, we used one type of remote sensing data, which corresponds to the Normalized Difference Vegetation Index (NDVI). NDVI was retrieved from Landsat 7 imagery, specifically derived from reflectances between Red (R) and Near Infrared (NIR) channels.

The Landsat 7 images covering our area of interest, corresponds to path 202 and row 38. These images were sourced from the USGS Earth Explorer website (https://earthexplorer.usgs.gov/), ensuring that the data used for our analysis is both accurate and reliable.

For our analysis, we used 15 satellite images acquired between 27/01 and 13/12 in 2003, and 10 images between 07/02 and 20/10 in 2004. NDVI values ranged from 0.3 to 0.66 in 2003, and from 0.39 to 0.61 in 2004. To generate continuous NDVI time series for our study period, we performed a linear temporal interpolation approach, to next derive leaf area index (LAI) and fc throughout the growing period of olive crop.

2.3. Models and adopted methodology

2.3.1. Model description

2.3.1.1. Two-Source-Energy-Balance (TSEB). The Two-Source Energy Balance (TSEB) model was first introduced by Norman et al. (1995), with former updates provided by Kustas and Norman (1999) and Kustas et al. (2004). The TSEB model generates two separate energy balance equations for soil and vegetation and calculates the sensible and latent heat fluxes by simultaneously resolving the two equations of continuity for turbulent fluxes and two energy balance equations (see Appendix A in Kustas and Norman, 1999; Norman et al., 1995):

$$Rn_s = G + H_s + LE_s \quad (1)$$

$$Rn_c = H_c + LE_c \quad (2)$$

$$H = H_s + H_c \quad (3)$$

$$LE = LE_s + LE_c \quad (4)$$

where the suffixes s and c stand correspondingly for "soil" and "canopy"; G is soil heat flux; H refers to sensible heat flux; and LE denotes latent heat flux; Rn corresponds to net radiation.

The TSEB model requires input data, such as meteorological data and canopy variables. Its primary inputs include two variables: Land Surface Temperature (LST) derived from measurements of thermal infrared (TIR) radiance, and vegetation fraction cover that modulates the distribution of energy between soil and vegetation. Radiative soil and vegetation temperatures were measured using two Infra-Red Thermometers (IRTS-Ps, Apogee), with a 3:1 field of view, at heights of 1 and 8.4 m respectively (Er-Raki et al., 2008; Hoedjes et al., 2007).

Radiometric surface temperature (Trad) is usually available at a single-view angle and is the combination of soil and vegetation temperatures in proportion to the respective fractions within the radiometer view, as follows (Kustas and Norman, 1999; Norman et al., 1995):

$$Trad = \left(fc \times T_c^4 + (1 - fc) \times T_s^4\right)^{\frac{1}{4}} \quad (5)$$

where Ts and Tc correspond to the soil and the canopy temperatures, respectively; fc is the fraction of the vegetation derived from the normalized difference vegetation index (NDVI) using the equation proposed by Gutman and Ignatov (1998).

The TSEB employs a set of equations that are solved iteratively (explained below) using a procedure developed by Norman et al. (1995). This procedure relies on a strong assumption, i.e., that the vegetation is not water-stressed and transpires at a maximum rate. The first estimate of canopy transpiration is provided by the Priestley-Taylor (PT) formulation (Priestley and Taylor, 1972) as follows:

$$LE_c = \alpha_{PT} \frac{\Delta}{\Delta + \gamma} Rn_c \quad (6)$$

where LE_c is the canopy latent heat flux (W/m^2); αPT is the Priestley-Taylor coefficient set to a standard value of 1.26; ϒ denotes the psychrometric constant and equals to 0.067 (kPa/°C); Δ is the slope of saturation vapor pressure-temperature relation (kPa/°C); Rn_c refers to the canopy net radiation (W/m^2). (Kustas and Norman, 1999; Norman et al., 1995)

$$H_c = \rho c_p \frac{T_c - T_a}{r_{ah}} \quad (7)$$

where H_c refers to the sensible heat flux from the canopy; T_a and T_c are the air and the canopy temperatures (K), respectively; r_{ah} denotes the aerodynamic resistance to heat transport ($s.m^{-1}$) based on the Monin-Obukhov similarity theory and is estimated following (Kustas et al., 2016); ρc_p is volumetric heat capacity of air ($J.m^{-3}.K^{-1}$).

After computing the initial estimate of LE_c, H_c is calculated as a residual term of the canopy energy-balance (Eq. (2)), T_c is obtained from H_c (Eq. (7)) and T_s is determined using Eq. (5). G flux is expressed as a constant fraction of Rns, which ranges from 0.2 to 0.5 according to Choudhury (1987) and Bastiaanssen et al. (1998), and LE_s is deduced as a residual term of the soil energy balance Eq. (1). If the canopy is transpiring at significantly less than the potential rate. The Eq. (6) results in an overestimation of LE_c, leading LE_s to become negative, indicative of condensation on the soil. This is unlikely during daytime conditions (unrealistic condition), and is considered as an indicator of system stress. Under such circumstances, the αPT coefficient is incrementally reduced using a sequential step-by-step method, suggesting that the canopy does not transpire at a maximum rate, until realistic daytime LE_c and LE_s ($LE_s \geq 0$) fluxes are computed. More information on the resolution procedure is available in (Anderson, 2012; Colaizzi et al., 2014; French, 2001).

2.3.1.2. Two-Source-Energy-Balance-Soil Moisture (TSEB-SM). In order to improve ET and its components, soil moisture (SM) in the 0–5 cm soil layer should be incorporated as an additional constraint, to improve the consistency between observed and simulated fluxes. Hence, a new model called ''TSEB-SM'' has been developed by Ait Hssaine et al. (2018).

TSEB-SM model calculates the turbulent fluxes by concurrently resolving the soil and canopy energy balance equations, similarly to the classic TSEB. However, by introducing data relative to 5 cm-top SM, the soil evaporation (E) term is better described, by adding a third resistance known as the soil surface resistance (r_{ss}), to the LE_s calculation formula, in addition to the soil and aerodynamic resistances.

Passerat de Silans (1986) proposed the following expression to compute the soil surface resistance to water vapor transfer:

$$r_{ss} = \exp\left(a_{rss} - b_{rss} \frac{\theta_{5cm}}{\theta_{sat}}\right) \quad (8)$$

with $\theta_{5\,cm}$ and θ_{sat} corresponding to 5 cm-top SM at actual and saturation levels, respectively; a_{rss} and b_{rss} are two empirical soil texture-dependent (dimensionless) coefficients, they were set to 8.2 and 4.3, respectively, in earlier studies (Sellers et al., 1992). In fact, no study has determined the respective values of these coefficients for each type of soil (Gan and Gao, 2015).

Ait Hssaine et al. (2018) proposed a calibration procedure to retrieve these two parameters for a dataset corresponding to a fraction of vegetation cover less than 0.5 (fc <=0.5), for which the soil is uncovered and hence ET is mostly driven by E. This condition (fc <=0.5) is not verified for the study site, thus arss and brss were assigned values of 5.67 and 1.4, respectively, which correspond to those found by Ait Hssaine et al. (2018) for a flood-irrigated site. These values are presumed to be identical to those of our study site, since they were identified for a site belonging to the same basin, with a similar soil type, identical irrigation system, and exposed to similar climatic conditions.

The TSEB-SM model calculates LE_s flux as follows (Ait Hssaine et al., 2018):

$$LE_S = \frac{\rho c_p}{\Upsilon} \frac{(e_s - e_a)}{r_{ah} + r_s + r_{ss}} \quad (9)$$

where LE_s is the soil latent heat flux (W/m^2); ρc_p is the volumetric heat capacity of air ($J.m^{-3}.K^{-1}$); ϒ denotes the psychrometric constant and equals to 0.067 (kPa/°C); e_s and e_a stand for the saturated vapor pressure at the soil surface and the air vapor pressure, respectively; r_{ah} represents the aerodynamic resistance to heat transport ($s.m^{-1}$); r_s refers to the resistance to heat flux in the boundary layer immediately above the soil surface ($s.m^{-1}$); r_{ss} is the top-5 cm soil surface resistance to water vapor transfer ($s.m^{-1}$).

The particularity of the TSEB-SM model relies on the calibration of the αPT coefficient, which has been modified in response to the SM in the root zone during the crop growing season. Further details on the TSEB-SM model and calibration strategies can be found in Ait Hssaine et al. (2018) and Ait Hssaine et al. (2020).

2.3.2. Methodology used

2.3.2.1. Sap flow data processing. Sap flow measurements need to be scaled in order to be representative of the field of interest. For this purpose, the daily volumetric sap flow (L/day) was initially adjusted to reflect the daily tree transpiration T (mm/day). This adjustment involved dividing the daily flux (L/day) by the average ground coverage of each tree, which was determined to be 45 m^2. More comprehensive details are provided in Er-Raki et al. (2010) and Williams et al. (2004). Moreover, the methodology for extrapolating sap flow measurements to account for the entire tree has also been employed in a similar manner by Cammalleri et al. (2013b) and Puig-sirera et al. (2021) over an irrigated olive grove. Then, the tree T is extrapolated to the stand-level T, which is representative of the experimental field scale (Er-Raki et al.,

2010). The T of a single tree is extrapolated to the field scale using the ET measurements from the EC tower. This extrapolation method was previously suggested by Williams et al. (2004) when scaling stand-level T. To do so, we assume that during dry conditions (when E is negligible), the relationship between field scale ET and tree T results from the scaling errors in tree T.

To identify the dry period, we track the evolution of the surface SM difference Δθ at 5 cm depth between two consecutive days. Once Δθ stabilizes and approaches zero, the corresponding SM is regarded as a threshold and E to be negligible when SM at 5 cm is lower than this threshold value. Further details concerning this approach can be found in Er-Raki et al. (2010).

Following the selection of dry conditions, a linear regression between the daily scaled sap flow and the total daily ET measured by the EC system (Fig. 2) is established. This upscaling is used to calculate the stand-level (field scale) T for the remaining wetting days of sap flow measurements (Er-Raki et al., 2010). We assume that the predominant wind speed and direction were identical between the dry (calibration period) and wet periods, so that the derived regression is applicable for wetting days (post-irrigation period), and the difference between total ET flux measured by EC system and scaled olive T reflects the contribution of E to total ET within the EC flux footprint (Williams et al., 2004). Next, these scaled sap flow values are used to evaluate the performance of TSEB and TSEB-SM models in terms of partitioning evapotranspiration into T and E.

2.3.2.2. Derivation of daily values of the αPT coefficient. The PT method (Priestley and Taylor, 1972) assumes that the equilibrium term, which corresponds to the radiative term of the Penman-Monteith (PM) equation, is much greater than the aerodynamic contribution, simplifying thus the Penman's expression of ET (Penman, 1948). According to this premise, the PT formulation for ET is expressed as:

$$ET = \alpha PT * Eeq \tag{10}$$

where Eeq is the equilibrium term, defined by Slatyer and McIlroy (1961) as the limit reached over a long fetch when unsaturated air comes into contact with a moist surface; αPT denotes the Priestley–Taylor coefficient.

The literature states that the αPT coefficient can vary significantly depending on crop type and climatic conditions. For perennial ryegrass, Davies and Allen (1973) obtained αPT values ranging from 1.01 to 1.34 with a mean value of 1.27. Jury and Tanner (1975) observed that for an irrigated potato crop, αPT was about 1.28 for a wet year and 1.57 for a dry year. Kanemasu et al. (1976) proposed αPT values of 1.28 for sorghum and 1.45 for soybean.

As SM declines, surface resistance to ET rises and the αPT coefficient drops (Flint and Childs, 1991; Raupach, 2000). Therefore, to avoid the use of a standard value of 1.26, which does not obviously reflect the local conditions of the Agdal site and does not account for advective conditions, we use the approach proposed by Flint and Childs (1991) for non-potential conditions, to deduce αPT throughout the growing periods of olive trees. This approach relies on actual evapotranspiration ET measured by the EC system and equilibrium evaporation (Eeq) that is independent of wind speed and based on air temperature and available energy (Flint and Childs, 1991).

$$\begin{cases} ET = \alpha PT * Eeq \\ Eeq = \dfrac{\Delta(Rn - G)}{\Delta + \Upsilon} \end{cases} \tag{11}$$

The αPT deduced from Flint and Childs (1991) stands for a bulk (system) coefficient, and thus reflects the contribution of E and T. Thus, to account for the effect of vegetation transpiration on global ET, we implement the approach suggested by Tanner and Jury (1976) and calculate the modified αPT coefficients for soil and vegetation using the following formula (Eq. 12): (Tanner and Jury, 1976)

$$\begin{cases} \alpha s = \begin{cases} 1 & (for\ \tau \le \tau 0) \\ \alpha PT - \dfrac{(\alpha PT - 1)(1 - \tau)}{(1 - \tau 0)} & (for\ \tau > \tau 0) \end{cases} \\ \alpha c = \dfrac{(\alpha PT - \alpha s * \tau)}{(1 - \tau)} \end{cases} \tag{12}$$

The subscripts s and c stand for soil and canopy, respectively. α_s and α_c are Priestley-Taylor coefficients for soil and vegetation, respectively. The αPT coefficient is calculated from the Flint and Childs (1991) equation (Eq. 11) on a daily timescale (between 09h00 and 17h00). The coefficient τ refers to a canopy transmission factor, which corresponds to the ratio of Rns to the total Rn. The coefficient τ is calculated using LAI and an extinction coefficient (kapa) (Campbell and Norman, 1998; Kustas and Norman, 1999). The variable τ0 is a threshold value of τ beneath which the canopy is dense enough so that E is close to equilibrium. The precise value of τ0 is not critical, and it can range from 0.2 to 0.5 (Agam et al., 2010; Tanner and Jury, 1976). A value of τ0= 0.3 is adopted for the present study, according to Agam et al. (2010).

To maintain the same rationale for the original TSEB model when setting a first approximation of latent heat flux for vegetation canopy, the annual average value of the α_c coefficient was used to run TSEB-CPT (computed αPT) model. We use these averaged values rather than the potential value of the αPT coefficient since the latter does not reflect semi-arid conditions of the study site.

2.3.2.3. Assessment of model performance. Daytime measurements of ET (from 9:00 a.m. to 5:00 p.m.) were used to assess the performance of three versions of TSEB in simulating ET, namely TSEB-SPT (standard αPT, run with the standard coefficient of 1.26), TSEB-CPT (computed αPT, performed with the annual average value of the calculated αPT), and TSEB-SM (the αPT coefficient is calibrated on a daily basis using a cost function).

Regarding ET partitioning, half-hourly sap flow data (from 9:00 a.m. to 5:00 p.m.) were aggregated at the daily timescale, and scaled to the

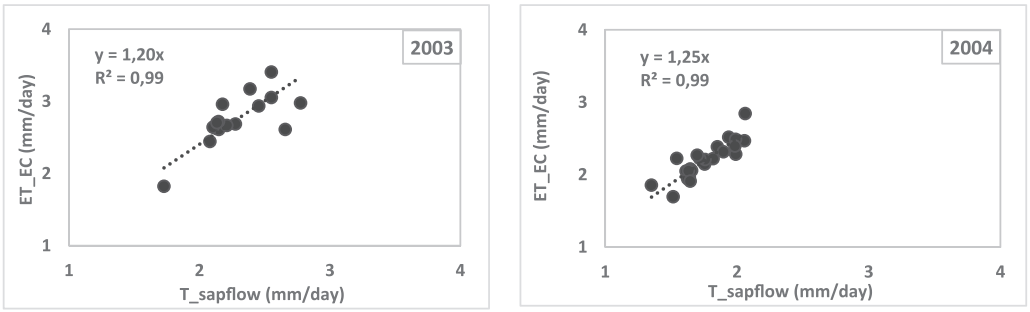

Fig. 2. Linear regressions between daily sap flow measurements and ET measured by the Eddy-Covariance system during the summer period of 2003 (left) and 2004 (right).

EC tower's footprint, then used to evaluate the performance of the three models in estimating the T component. The semi-hourly values of simulated E by the three versions of TSEB were aggregated at the daily timescale and then compared against the measured ones, in order to assess how well the three models performed in terms of the E component estimation. Estimates of E are beforehand derived by subtracting the scaled sap flow T from the measured ET by EC system. This method was also applied by Rafi et al. (2019) for a drip-irrigated wheat crop, and Cammalleri et al. (2013b) over an irrigated olive orchard.

The intercomparison of the effectiveness of each model is quantified using three statistical metrics, including: the coefficient of determination (R2), the root mean square error (RMSE) and the mean bias error (MBE) between simulated and observed fluxes.

$$RMSE = \sqrt[2]{\frac{\sum_{i=1}^{n}(y_i - x_i)^2}{n}} \quad (13)$$

$$MBE = \frac{\sum_{i=1}^{n}(y_i - x_i)}{n} \quad (14)$$

$$R^2 = 1 - \frac{\sum_{i=1}^{n}(y_i - x_i)^2}{\sum_{i=1}^{n}(x_i - \hat{x})^2} \quad (15)$$

Where y_i *and* x_i are modeled and observed values, respectively; n is the number of available observations; $\hat{x}$ is the mean of observations.

3. Results & Discussion

This section includes an analysis of the temporal variability of the αPT coefficient at our study site during two growing periods, followed by a discussion of the performance of the three versions of TSEB model in estimating ET at various time scales (semi-hourly, daily and monthly), and concludes with an assessment of their ability to partition ET into T and E.

3.1. Analysis of the variability of daily αPT values

Time series of the daily average values of the αPT coefficient are generated throughout the growing seasons of 2003 and 2004 (Fig. 3). The values of αPT fluctuate between 0.34 and 1.25 during the 2003 growing season, and from 0.38 to 1.21 in 2004 with an annual average value reaching 0.75. It is worth reminding that the Agdal site is irrigated by flood irrigation, with a water supply of 100 mm for each irrigation event. Thus, peaks in the αPT coefficient are observed after irrigation events, in accordance with the redistribution of SM in the soil profile from the surface to the root zone. The fluctuation of αPT is significantly impacted by the temporal variation of SM level and VPD. Thus, the highest value of the αPT occurs after a wetting event (irrigation or/and rainfall), associated with a strong evaporative demand corresponding to large VPD. Conversely, the lowest value of the αPT occurs after a drop in SM and an increase in the evaporative demand.

To distinguish between contributions from olive trees and from bare soil in the bulk αPT coefficient, we calculate the α_c coefficient for olive trees by using Eq. (12). The average annual value of the α_c coefficient is equal to 0.58 and 0.57, respectively for 2003 and 2004, which is close to the average annual value of the computed αPT coefficient of the system (canopy and soil). Fig. 4 illustrates the dependency of VPD and α_c under various ranges of root zone SM throughout [15 May - 05 June] 2003 and [20−29] August 2003. Actually, the root system depth of olive trees ranges from 60 to 80 cm (INRA Meknès Magazine, 2016). Also, according to Table 22 in FAO-56 (Allen et al., 1998), the maximum effective depth of root system for olive trees (40–60% ground coverage by canopy) is between 1.2 and 1.7 m. Thus, because SM measurements available at the field scale were taken at a maximum depth of 40 cm, SM at this corresponding depth is considered to be representative of the root

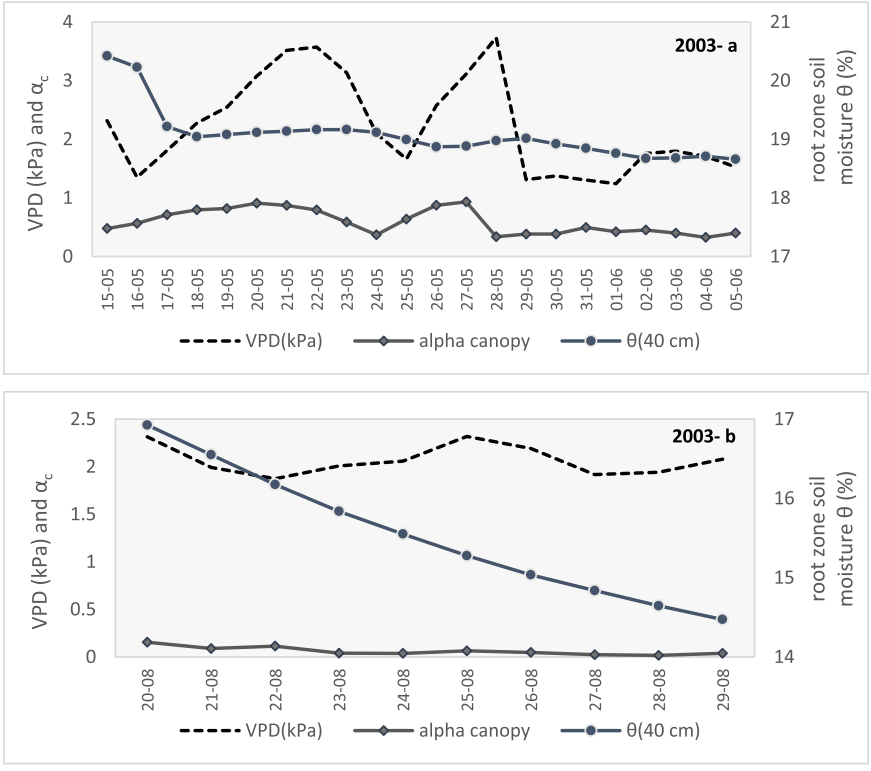

Fig. 4. Dependency of canopy Priestly-Taylor coefficient αc to VPD under different ranges of root zone soil moisture in Agdal site 2003. We consider the case of available moisture (θWp ≤θ) (a) and the case of root zone moisture below the wilting point (b).

zone SM. We analyze the case of available SM (energy-limited conditions), considering for instance an average daily SM of the root zone that fluctuates between 21% and 18% with **θ_{fc}=32% and θ_{Wp}= 19%** according to the pedotransfer function proposed by Wösten (1997). We note that the α_c coefficient rises as the VPD increases, and α_c values range from 0.3 to 0.9, with a VPD varying from 1.2 to 3.7 kPa. Hence, high levels of VPD (>1 kPa) promote tree transpiration by inducing a greater moisture gradient between leaves and atmosphere. Nevertheless, high VPD can trigger a greater stomatal resistance to conserve water for SM levels θ close to or below the wilting point θ_{Wp} ($14 \leq \theta \leq 17\%$), as illustrated in Fig. 4(b). Therefore, trees acclimate to moisture deficits by reducing T rates, resulting in a decrease in α_c coefficient (Baldocchi and Xu, 2007).

3.2. Model performance for ET simulations at the half-hourly timescale

Fig. 5 displays the measured and simulated latent and sensible heat fluxes by the TSEB-SPT, TSEB-CPT and TSEB-SM. The performance of the Two-Source Energy Balance (TSEB) models was evaluated over two growing seasons of 2003 and 2004 at the Agdal site. The results revealed significant disparities in the model's accuracy and reliability in estimating latent (LE) and sensible (H) heat fluxes.

The TSEB-SPT model tends to overestimate LE fluxes, with a R^2 coefficient of 74% and 55%, and an RMSE around 159 and 187 W/m^2, respectively, for the growing seasons of 2003 and 2004. This overestimation subsequently lead to the underestimation of H fluxes, evidenced by lower R^2 values of 14% and 12%, and an RMSE evaluated at 159 and 192 W/m^2, respectively. The overestimation of LE is mainly related to the preset value of αPT coefficient (αPT=1.26), which corresponds to a typical evaporative demand without any particular aerodynamic components, and that disregards the effect of water vapor deficit on ET. However, this value decreases when the trees are water-stressed.

Enhancements were noticed with the TSEB-CPT version, which incorporates a site-specific annual average value of the α_c coefficient calculated for the Agdal site, during 2003 and 2004, in order to account for actual environmental conditions (Fig. 5). This adjustment improved the estimation of LE and H fluxes. Indeed, RMSE and MBE are considerably reduced for LE: during the 2003 and 2004 growing seasons. Thus, RMSE drops from 159 to 47 W/m^2, and from 187 to 57 W/m^2, respectively, while MBE declines from 144 to 22 W/m^2, and from 167 to 6 W/m^2, for the respective years. Furthermore, estimates of H flux are drastically enhanced. For 2003 and 2004 growing seasons, R^2 between simulated and observed H increases to 68% and 67%, respectively, while RMSE decreases from 159 to 47 W/m^2, and from 192 to 57 W/m^2, respectively.

TSEB-CPT model tends to globally overestimate the latent heat fluxes, particularly for LE<300 W/m^2, and the H flux values are slightly underestimated as a result of this overestimation. The balance between the simulated and observed values of LE and H fluxes results from the energy balance closure for the soil-vegetation system, given that Rn and G are set to their measured values. The discrepancies between the modeled and measured LE and H fluxes are primarily induced by the setting of the α_c coefficient to a single value, whereas this coefficient fluctuates on a daily basis according to Fig. 3 and Fig. 4. Our findings underscore the importance of adjusting the α_c coefficient to account for daily climatic variations and soil water content for improved accuracy.

For the TSEB-SM version, which integrates SM as an additional input, we note that this model version outperformed the original TSEB-SPT in estimating both LE and H fluxes, for the two selected periods at the Agdal site (Fig. 5). Also, TSEB-SM produces lower MBE than TSEB-CPT and exhibits a slight underestimation of LE and overestimation of H fluxes. For 2003 and 2004, MBE is about −5.5 and 0.3 W/m^2, respectively, for LE values, and about 10.3 and 4.3 W/m^2, respectively, for H estimates. Regarding RMSE, we note almost similar values for both models (TSEB-CPT & TSEB-SM). However, there is a significant dispersion in the LE flux estimates provided by the TSEB-SM model, particularly in 2004. Larger discrepancies within the scatterplot correspond to dates for which 9 m-height wind speed exceeds 3 m/s. Since the calculation of E in the TSEB-SM model involves aerodynamic and soil resistances, which are low during these corresponding dates, the simulated E values are larger than the actual ones, given the low SM levels at the top 5 cm. Consequently, the simulated contribution of E to total ET is large, which results in large values of simulated ET.

3.3. Model performance for ET simulations at the daily timescale

For a comparison purpose, Fig. 6 displays times series of LE daily values estimated by TSEB-SPT, TSEB-CPT and TSEB-SM, along with times series of LE daily values measured from the EC tower, within the Agdal site throughout the olive tree growing seasons of 2003 and 2004. We note that days with missing LE values between 9:00 and 17:00 were excluded from this analysis.

Our comparison of three TSEB model versions: TSEB-SPT, TSEB-CPT, and TSEB-SM, against observed daily ET demonstrates that all models display comparable temporal patterns, adeptly reproducing daily ET peaks during the two consecutive growth seasons. The daily values of measured ET vary between 1.2 and 4.1 mm in 2003 and range from 1.1 to 4.7 mm in 2004. In contrast, the simulated ET fluxes by TSEB-SPT, TSEB-CPT and TSEB-SM range from 1.8 to 5.5 mm, from 1.0 to 3.8 mm, and from 1.4 to 4.1 mm in 2003, and range from 2.0 to 5.9 mm, from 1.1 to 4.1 mm, and from 0.9 to 4.5 mm in 2004, respectively.

Overall, TSEB-SPT model frequently overestimates daily ET values throughout the entire two growing periods, whereas TSEB-CPT and TSEB-SM models were more closely aligned with the corresponding actual ones during certain periods of the year. Indeed, the discrepancies between observed and simulated fluxes of daily ET are slightly low and stable (1) for TSEB-CPT model in March 2003 and from March to mid-May 2004, (2) for TSEB-SM, from March to April 2003, and between April and mid-June 2004. Over 2003, ET peaks are common, with maximum values during the months of May, July, and August reaching 4.1 mm on 21/05. Over 2004, ET maxima are observed in June and July, with a high value of 4.7 mm recorded on 26/06.

The dynamics of daily ET measured by the EC tower are well tracked by the three TSEB versions, with daily ET dynamics, influenced by changes in Rn, VPD and SM levels at 5 cm and 40 cm depths. Nevertheless, both versions (TSEB-CPT & TSEB-SM) frequently underestimate ET fluxes, particularly during periods following wetting events (mainly irrigation or substantial rainfall). As stated previously, the study site is flood-irrigated with a water supply of 100 mm per irrigation event. With this irrigation method, SM rapidly increases and can potentially exceed SM at field capacity. Under such saturated soil conditions, the differences between simulated and actual ET fluxes are significant for both models, particularly for TSEB-SM.

3.4. Model performance for ET simulations at the monthly timescale

Fig. 7 displays the performance of TSEB-SPT, TSEB-CPT and TSEB-SM at the monthly timescale, on the basis of a Taylor diagram that provides a concise overview of the correspondence degree between measurements and simulations (Taylor, 2001). For LE and H fluxes, the correlation coefficient (r), the centered root mean square difference (RMS) and the ratio of standard deviations are indicated by single-points on the two-dimensional (2-D) graph. By combining these statistical metrics, one may easily assess the degree of pattern correspondence and determine how well a given model simulates measurements. Further details on the diagram and its interpretation are provided in Taylor (2001). Metrics related to TSEB-SPT, TSEB-CPT, and TSEB-SM are indicated using triangles, circles, and rectangles, respectively. Reference measurements are indicated using green rectangles. The distinct colors denote the growing period of olive trees between March and November. The radial distances are proportional to the model standard deviations,

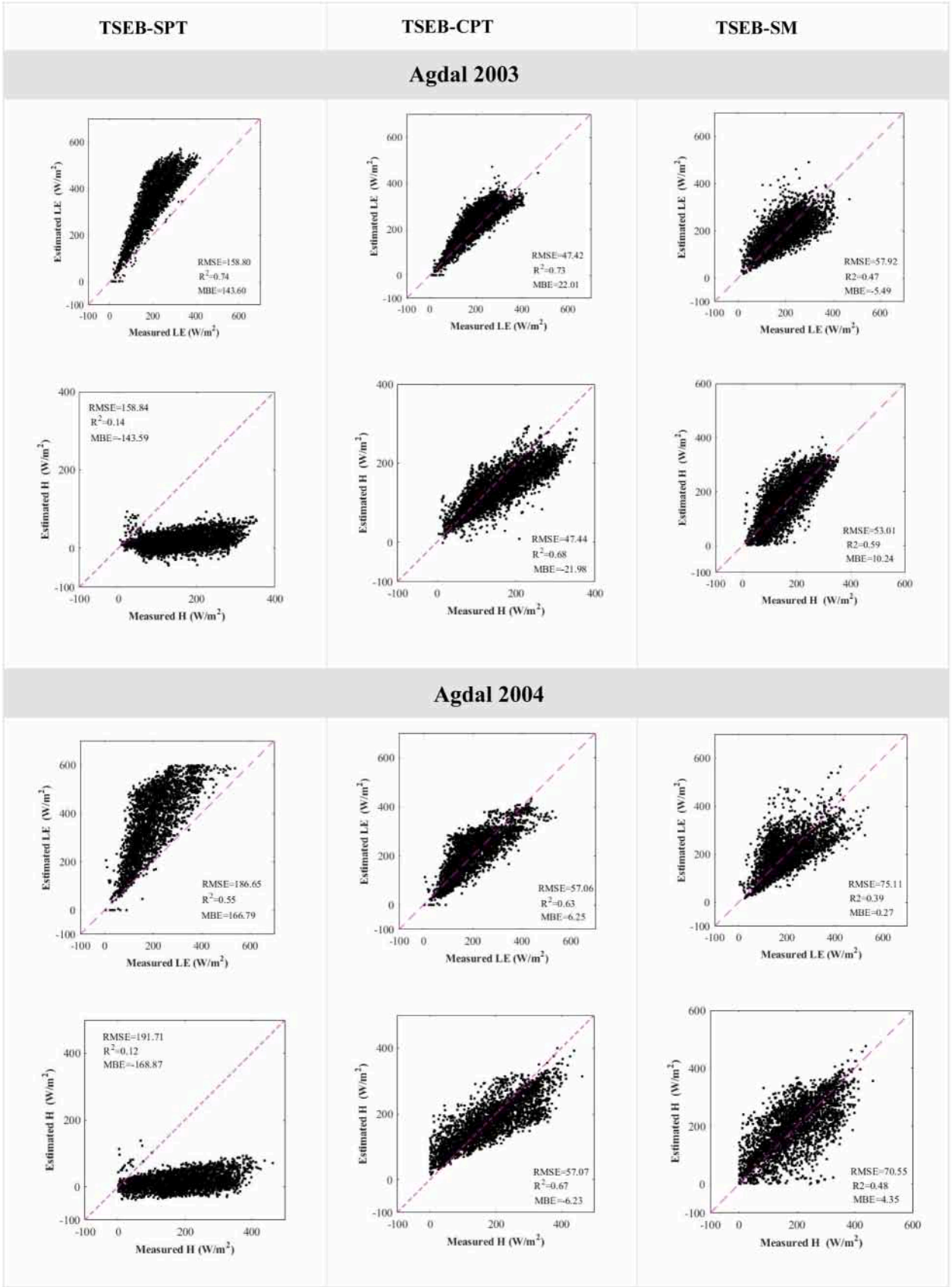

Fig. 5. Scatterplot of simulated versus measured latent (LE) and sensible (H) heat fluxes at the half-hourly timescale, for the Agdal site, using the TSEB-SPT (left), TSEB-CPT (center) and TSEB-SM (right) models during the 2003 and 2004 growing seasons.

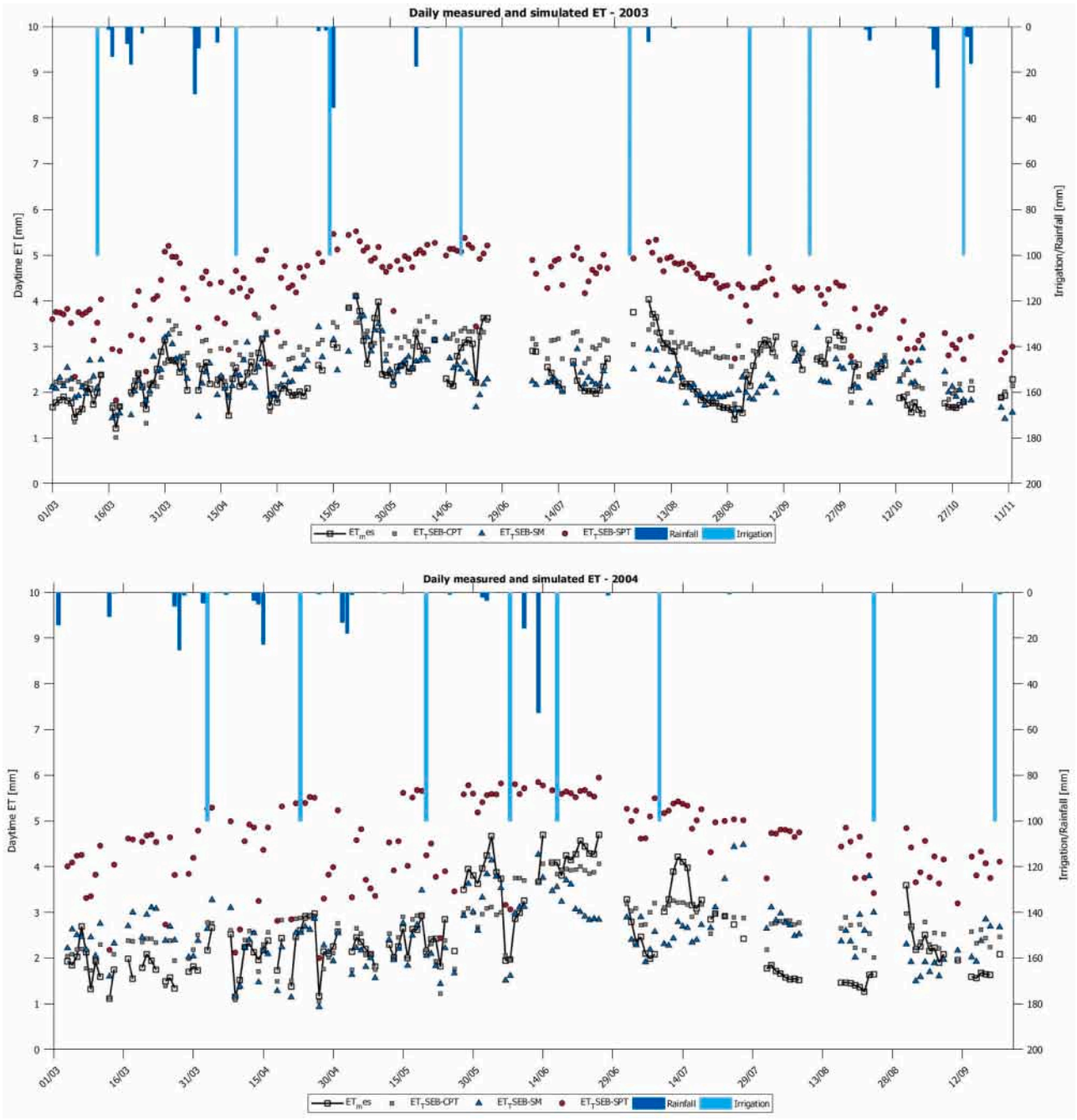

Fig. 6. Daily values of ET simulated by TSEB-SPT, TSEB-CPT and TSEB-SM models compared to daily measured ET by the EC system at Agdal orchard during 2003 (top) and 2004 (bottom).

and the green dashed semi-circles indicate the RMS error. The correlation coefficients between simulations and measurements are indicated by the azimuthal positions.

Taylor diagram reveals that the correlation coefficients (r) fluctuate between 0.6 and 0.9, indicating a moderate to high level of agreement between the measured and simulated LE values across all models during the two seasons 2003 and 2004.

In 2003, TSEB-SPT consistently overestimates LE measurements all months. This overestimation is indicated by a standard deviation reaching 110 W/m^2 and RMS fluctuating between 50 and 70 W/m^2. Conversely, TSEB-CPT and TSEB-SM models exhibit lower standard deviation values varying between 35 and 71 W/m^2, while RMS ranges from 28 to 42 W/m^2, and from 42 to 56 W/m^2, respectively. Furthermore, both models slightly overestimate LE fluxes, with best performance achieved in March, April, October, and November (RMS is around 28 W/m^2 for TSEB-CPT and 42 W/m^2 for TSEB-SM).

In 2004, TSEB-SPT shows standard deviations from 110 to 150 W/m^2, and RMS from 88 to 110 W/m^2 when simulating LE fluxes. Besides, TSEB-CPT and TSEB-SM perform similarly, with slightly lower RMS for TSEB-CPT (between 34 and 50 W/m^2) as compared to TSEB-SM (from 34 to 66 W/m^2). Good estimates of both models are noticed in April and May. Overall, our results suggest that the TSEB-CPT model reproduces better the total evapotranspiration at the monthly timescale.

The olive tree's annual growth cycle runs from March to November, during which it goes through several phenological phases from inflorescence development to fruit ripening and harvest (Sanz-Cortés et al., 2002). The most intense period of the annual cycle is from March to June. During this phase, the olive tree's water requirement is at its

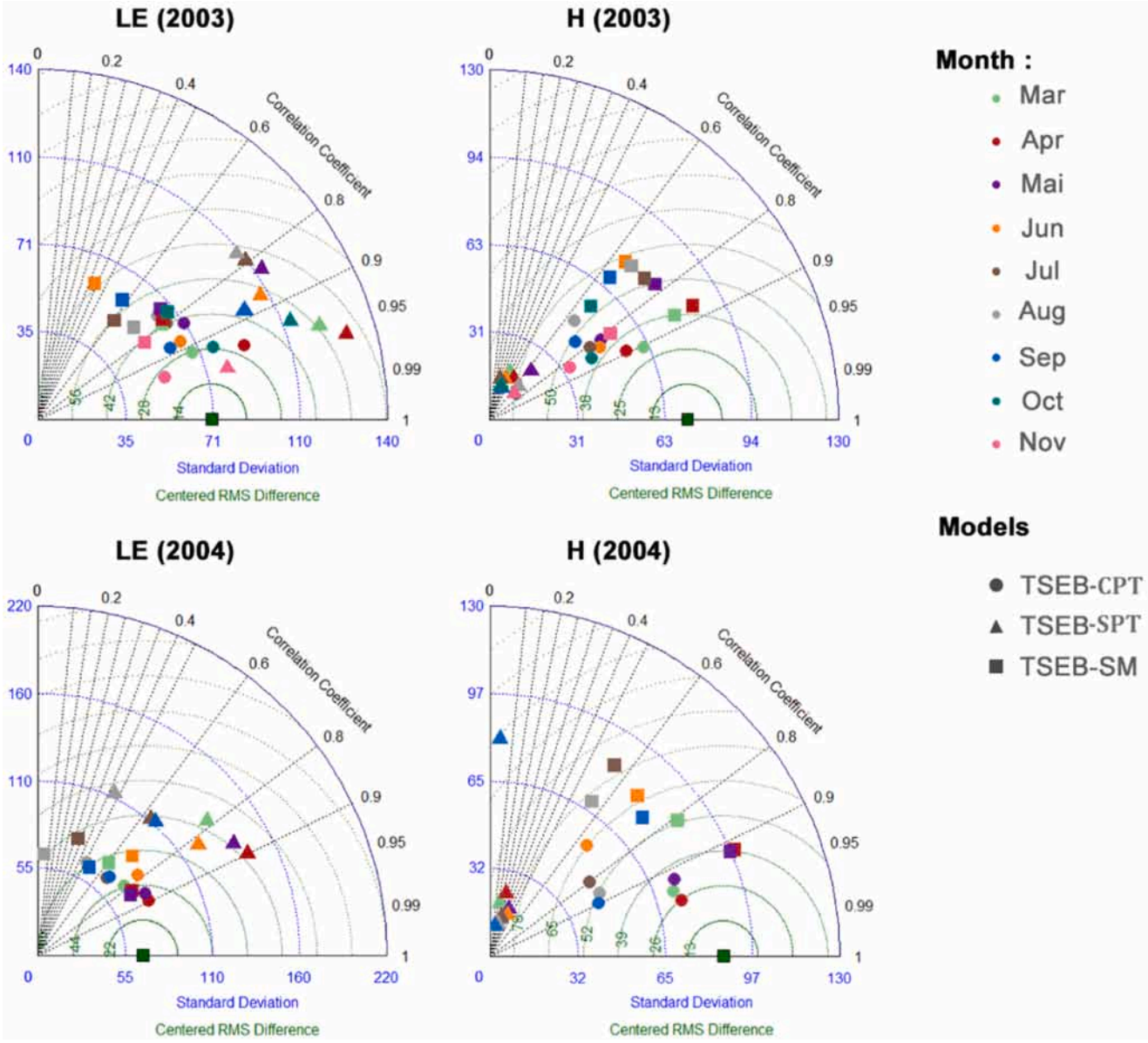

Fig. 7. Taylor Diagram for sensible (H) and latent (LE) heat fluxes simulated by TSEB-SPT, TSEB-CPT and TSEB-SM models at a monthly timescale in 2003 and 2004.

highest (Carr, 2013; Sanz-Cortés et al., 2002; INRA Meknès Magazine, 2016). This is corroborated by our LE measurements and their corresponding simulated values by the three versions of TSEB during this period for 2003 and 2004 growing seasons. For instance, in 2003, the average monthly ET measured from March to June (from 9:00 a.m. to 5:00 p.m.) was 75 mm, compared to 66 mm from July to November. The corresponding average ET simulated by TSEB-SPT/ TSEB-CPT/ TSEB-SM models for the former period reached 133/84/76 mm, and for the latter 110/72/61 mm, respectively.

In semi-arid regions similar to our study area, the amount of contribution of each vegetation species to soil-surface interactions varies throughout the year according to their differing phenological stages (Luo et al., 2018). For heterogeneous vegetation cover layers, trees and the underneath soil, as well as the understory layer (weeds or natural grass), interact throughout the growing period and all contribute to turbulent and radiative exchanges (Baldocchi et al., 2004). Few studies have assessed the performance of the TSEB model on perennial crops and natural permanent vegetation (Andreu et al., 2018; Cammalleri et al., 2010; Guzinski et al., 2013). Our findings are consistent with earlier studies regarding the estimation of LE, and the magnitudes of errors associated with TSEB-CPT and TSEB-SM simulations are comparable to the error boundaries established in other energy balance model studies. For instance, Boulet et al. (2015) investigated various dual-source model schemes, and reported that the RMSD for LE in irrigated and rain-fed wheat fields ranged from 53 to 73 W/m^2. Likewise, Timmermans et al. (2007) contrasted the performance of TSEB model against the SEBAL (Surface Energy Balance Algorithm for Land) model on a sparsely vegetated grassland and pasture area, and obtained RMSD values for LE of 62 and 70 W/m^2, respectively for both sites. Additionally, Burchard-Levine et al. (2020) proposed TSEB-2S (two season) to account for two key phenological periods in a semi-arid tree-grass ecosystem, depending on when the grass layer is active (grass-soil system) and when it becomes senescent (tree-soil system), without introducing additional variables or altering the model's fundamental structure. They revealed that the TSEB-2S model improved LE estimates compared to the default configuration of TSEB, with RMSD values ranging from 57 to 63 W/m^2. Similarly, Andreu et al. (2018) assessed the effectiveness of TSEB for simulating surface energy fluxes over savanna landscape, which exhibits numerous similarities with other wooded Mediterranean coverages, including olive groves and vineyards.

They carried out several wind profiles and different roughness patterns in the TSEB model and reported errors for simulated LE varying from 44 and 60 W/m^2.

On the other hand, the sensible heat flux H is largely undervalued by the TSEB-SPT model owing to the overestimation of LE during the whole growing season, with RMSD values for H spanning between 65 and 91 W/m^2 for 2003 & 2004 simulation periods. The TSEB-CPT version improved the simulation of H fluxes, but they remain slightly underestimated with RMSD values fluctuating between 25 and 50 W/m^2, and the most accurate simulations were reported in March and April. Unlike TSEB-SPT and TSEB-CPT versions, estimates of the sensible heat flux H were improved by TSEB-SM model throughout 2003 and 2004 growing seasons, this is likely due to the robustness of the iterative procedure proposed by Ait Hssaine et al. (2018) for estimating soil and vegetation temperatures, which is based on the minimization of the cost function of soil and vegetation energy balance equations. However, H estimates were overall slightly overestimated, and RMSD values ranged from 38 to 78 W/m^2, with the most precise estimates of H occurring in March and April of 2003 and in April and May of 2004. Feng et al. (2023), indicated also a modest overestimation of H flux by the TSEB model over a semi-arid orchard by altering soil resistance coefficients and incorporating the heat transfer resistance (kB^{-1}) parameterization scheme into the original model, in an attempt to optimize the latter's performance in estimating turbulent fluxes.

The underestimation of H is systematic in the original TSEB model and has been reported in several studies (Andreu et al., 2018; Burchard-Levine et al., 2020; Cammalleri et al., 2010; Chirouze et al., 2014; Li et al., 2019; Morillas et al., 2013). This underestimation of H may be attributed to several factors, including the overestimation of LE fluxes, and the use of standard parameters in the formulation of the soil aerodynamic resistance in the original TSEB model as demonstrated by Li et al. (2019). Indeed, according to Morillas et al. (2013), TSEB underestimated H for high measured H rates over a semi-arid Mediterranean tussock grassland, with RMSD values of 64 and 84 W/m^2 using parallel and series resistance approaches, respectively. Furthermore, Kustas et al. (2016) conducted a subsequent analysis over the same semiarid grassland area and indicated that the significant bias in H estimates are caused by key vegetation inputs and semi-empirical coefficients of the soil resistance formulation used to estimate H_S flux. Through the adjustment of the soil resistance coefficients based on soil roughness measurements and vegetation features, Kustas et al. (2016) achieved precise results for this site. Similarly, Burchard-Levine et al. (2020), reported that a large underestimation of H flux were observed during the dry summer period (RMSD of 82 W/m^2) over a tree-grass semi-arid area, and attributed this to the vegetation layer parametrization within the TSEB model, which was not able to account for the significant phenological changes occurring in the vegetation layer during the summer. It is worth mentioning that H flux estimates may be improved by implementing alternative models of in-canopy wind profile, such as the Massman (1987) model within TSEB-SPT and TSEB-CPT versions. In fact, Cammalleri et al. (2010) reported that the Massman model yielded slightly better performance for an olive orchard.

3.5. Model performance for ET partitioning into T and E components

Tree transpiration (T) constitutes the most significant component of ET in irrigated olive orchards under semi-arid conditions (Zuñiga et al., 2014). As a result, determining T is a critical issue in order to apply proper irrigation scheduling. Fig. 8 depicts the daytime variation of actual T with those simulated by the three versions: TSEB-SPT, TSEB-CPT, and TSEB-SM. Overall, the simulated T by the three versions has the same temporal pattern than the measured T over the 32 and 102 days corresponding to the experimental periods of 2003 and 2004.

The daily measured T is evaluated at 62/128 mm, compared to 64/188 mm, 138/405 mm, and 17/114 mm estimated by TSEB-CPT, TSEB-SPT and TSEB-SM models, for the two respective years. Notably, the TSEB-SPT model largely overestimates the daytime T, with an RMSE of 2.41 mm in 2003 and 2.79 mm in 2004. This overestimation is mainly attributed to the use of a single αPT coefficient value of 1.26, which is incompatible with our experimental condition (see Section 3.1). Besides, the said model does not include a specific calibration of the αPT coefficient in response to stress conditions, underlying therefore the need for adjustment of this parameter.

Conversely, the T component is well reproduced by TSEB-CPT model in 2003, with an RMSE of 0.27 mm between simulations and observations. However, the discrepancy between simulated and measured T in 2004 is considered to be slightly significant, with an RMSE of 0.67 mm. Exceptions were noted during specific intervals, such as [13/07–20/07] or [26/08–09/09], where the model's simulations closely match the measurements. Regarding the TSEB-SM model, our results reveal a constant underestimation of simulated T during the whole summer period of 2003, with an RMSE of 1.41 mm. In 2004, the agreement between measured and modelled T is satisfactory between DOY 130 (09/05) and DOY 160 (08/06). Beyond this period, the gap between simulations and measurements increases resulting in an RMSE of 0.45 mm.

Our analysis emphasizes the importance of the αPT coefficient in estimating the T component. As previously mentioned, TSEB-CPT calculates the T component by using an averaged value of the αPT coefficient, which is equal to 0.58 in 2003 and 0.57 in 2004, whereas this coefficient is very sensitive to the variation of root zone SM, as well as the changes in VPD. In contrast, TSEB-SM adopts a dynamic approach to compute T by calibrating the αPT coefficient on a daily basis. This approach is based on a cost function designed to minimize the discrepancy between the simulated and measured surface temperature.

The gap between measurements and TSEB-CPT simulations of the T component is partially ascribed to the value of the αPT coefficient. Indeed, we compare the averaged αPT value used to run the TSEB-CPT model with that derived on a daily basis by inverting Eq. (6) that links the measured T (by sap flow sensors) to trees net radiation Rn_c, and that we call hereafter "$\alpha PT_{sapflow}$". We find that the $\alpha PT_{sapflow}$ values range from 0.51 to 0.98 in the summer of 2003, and are between 0.2 and 0.7 in 2004. As a result, the simulated T by TSEB-CPT is often larger than the measured one, particularly during the summer of 2004 (Fig. 8 & Fig. 9).

The calibration of the αPT in TSEB-SM model yields low values, less than 0.26 during summer period of 2003, and between 0.18 and 0.45 in 2004. This explains the low simulated T values by TSEB-SM, except for the time period from DOY 130 to DOY 160 in 2004, where T is accurately simulated, since the calibrated values of αPT coefficient are close to the measured ones (Fig. 9).

The disparity between T measurements and simulations can be also related to the fact that G flux is calculated as a fraction of Rn_s, whereas the conditions that drive the interaction between these two components is likely to change over the study period (Aguirre-García et al., 2021; Colaizzi et al., 2016; Santanello and Friedl, 2003). Furthermore, this fraction may vary according to both weather conditions and soil type, suggesting that the 0.5 chosen value may not be appropriate for the study site (Choudhury, 1987). This probably impacts the estimation of available energy for the canopy-soil system to some extent, resulting in an under- or over-estimation of LE flux. Besides, the three TSEB versions simulate both olive trees and understory vegetation T simultaneously, without distinguishing between the two components, while the measurements account for olive transpiration only. In addition, we note that the scaling approach is not flawless, which may contribute to the difference between simulated and measured T (Er-Raki et al., 2010; Fernaández et al., 2001; Williams et al., 2004).

Fig. 10 shows that the simulated E by TSEB-SPT is underestimated for the whole summer period, with an RMSE of 0.29 and 1 mm for 2003 and 2004, respectively. Also, TSEB-SPT and TSEB-CPT simulations of E show an inverse temporal trend with T. TSEB-CPT tends to overestimate E during the 2003 summer, with an RMSE of about 0.56 mm and an MBE of 0.50 mm, while it underestimates E in 2004, with an estimated RMSE

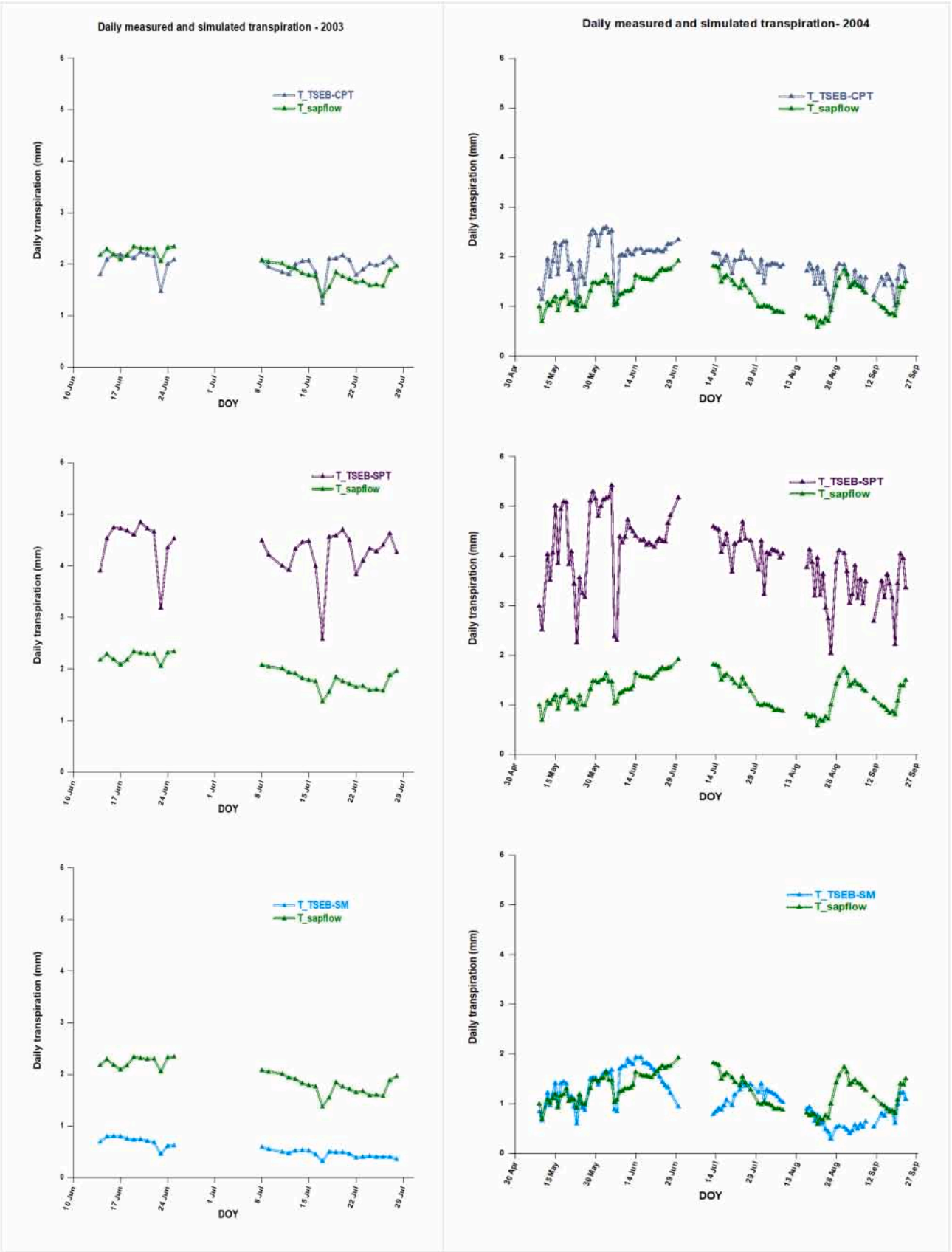

Fig. 8. plot of measured T by sap flow sensors and simulated ones by TSEB-CPT, TSEB-SPT and TSEB-SM, at daily timescale, during the summer period of 2003 (left) and 2004 (right).

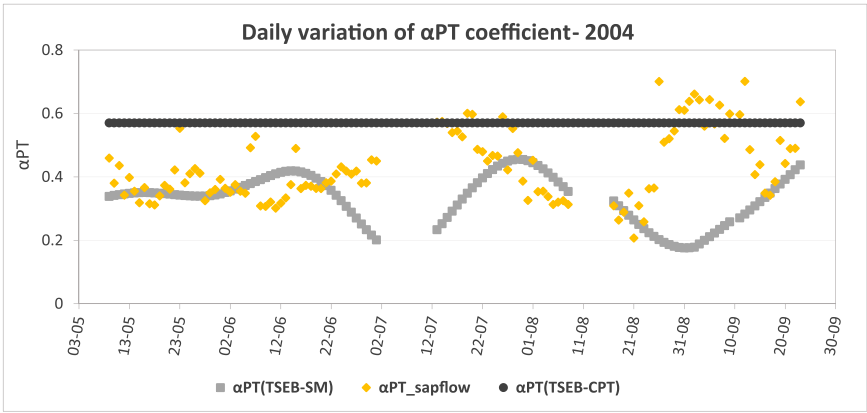

Fig. 9. plot of measured and simulated αPT coefficient, at daily timescale, during the 2004 summer period.

of 0.85 mm and a negative MBE of −0.55 mm.

Overall, the TSEB-SM simulations of E exhibit the same temporal variations as measured E, with delayed peaks and drops. TSEB-SM overestimates E, with RMSE and MBE values of 1.29 and 1.22 mm, respectively, in 2003. Conversely, it simulates well E between DOY 130 to DOY 160 in 2004, and slightly overestimates E with an MBE of 0.24 mm for the remaining period. TSEB-SM produces higher values of E than TSEB-SPT during the two summer periods, which increase the daily ET contribution from soil surface. Besides, the E estimates are large for some dates, although the corresponding SM levels at 5 cm depth are lower than the wilting point. This may be explained by the values of resistance terms included in the formulation of E, particularly the soil surface resistance r_{ss}. In fact, the empirical coefficients arss and brss used to calculate this term are not locally calibrated, since we assume that they are similar to those found by Ait Hssaine et al. (2018) for a flood-irrigated site, cultivated with wheat in the Tensift basin.

For the original TSEB, the underestimation of E can be assigned to the fact that this component is computed as a residual term and thus, affected by the overestimation of simulated LE_c flux. In addition, the standard formulation of aerodynamic resistance used in TSEB may not be appropriate for olive tree orchards. The large values of simulated soil temperature could also justify the underestimation of E component. In addition, the disparities between simulated and observed E fluxes can be partly related to errors in the scaling approach of sap flow measurements, which results in an under(over)-estimation of the measured E at the study site.

Several studies have demonstrated that TSEB model performs poorly in LE partitioning (Burchard-Levine et al., 2020; Kustas et al., 2019; Song et al., 2022). As demonstrated in Burchard-Levine et al. (2020), LE fluxes were well simulated by TSEB-2S (two season) over a tree-grass ecosystem for different years and sites. Nevertheless, when comparing simulated E to lysimetric measurements, biases were identified, indicating that the partition of LE was imprecise (Burchard-Levine et al., 2020). Song et al. (2022) found that TSEB model produced a higher T/ET ratio than the water use efficiency (WUE) approach (Zhou et al., 2016), particularly during crop senescence.

This could be related to the fact that the soil and vegetation flux partitioning in the TSEB model is heavily dependent on the fraction of green vegetation (fg), as well as LAI values (Kustas et al., 2019). Moreover, Häusler et al. (2018) evaluated the TSEB's performance in terms of ET partitioning over an intensive olive orchard, using medium-resolution satellite imagery, and the findings showed that the daily values of T and E were under- and over-estimated, respectively. As pointed out by Kustas et al. (2019), further investigations need to be undertaken to assess whether the poor partitioning of TSEB is related to uncertainties in the input values or to biases resulting from the modeling structure. In contrast to our findings, Song et al. (2022) demonstrated the effectiveness of TSEB-SM regarding ET partitioning over different land covers, and stated that the highest discrepancy of T/ET estimated from the TSEB-SM model occurred during the period of decline in plant cover, particularly at the end of the growing season. Nevertheless, the T/ET divergence remains lower when compared to the original TSEB, since the T algorithm was not affected by the value of the fraction of fg (Song et al., 2022). On the other hand, E demonstrated a temporal tendency opposite to T, as E would display large variation at the beginning of the growing season owing to wetting and drying cycles produced by water supply (irrigation/rain). However, E would progressively decrease as leaf area arose. Song et al. (2022) discovered that the TSEB and TSEB-SM models produced similar E values for irrigated cropland, whereas for desert steppes and shrub forests, the TSEB-SM model yielded higher E values.

4. Conclusion

As part of the current work, we assessed the performance of three versions of TSEB model in simulating ET and estimating its components (soil evaporation E and plant transpiration T) over a semi-arid olive orchard, at various timescales. These models include: (i) the original TSEB with a standard αPT coefficient (TSEB-SPT), (ii) with a computed one (TSEB-CPT), and (iii) the TSEB-SM that requires SM data to further constrain soil evaporation. According to our findings, the TSEB-SPT model is likely to produce larger errors at semi-hourly scale in predicting ET flux and its components T and E. These errors could be amplified under strongly advective conditions. The TSEB-CPT and TSEB-SM models enhance ET estimates and yield better agreements with reference measurements, including lower errors (with an average relative value of 24%) and better correlation between simulated and observed ET for TSEB-CPT model. Additionally, both modeled and observed values of daily ET exhibit comparable temporal patterns, and the peaks of daily ET are well captured by the three TSEB versions. Nevertheless, TSEB-CPT and TSEB-SM versions frequently underestimate ET fluxes during periods following wetting events. As for monthly timescale, the TSEB-CPT model reproduces better the total ET.

Regarding the partitioning of ET into T and E, the simulated T values by TSEB-SPT showed discrepancies from sap flow measurements, highlighting the necessity for precise canopy αPT coefficient inputs derived from EC measurements to improve accuracy.

While TSEB-SM provides lower values of T component due to lower values of canopy αPT coefficient, revisiting the calibration function of this coefficient within the context of arboriculture (woody species) is recommended. Future studies should focus on determining αPT coefficient for perennial woody crops, and examine its variability on daily and shorter time spans, as well as link its fluctuations to variations in VPD and soil water availability, with the purpose of enhancing estimates of T component.

Furthermore, TSEB-SM generates higher E values, although for some

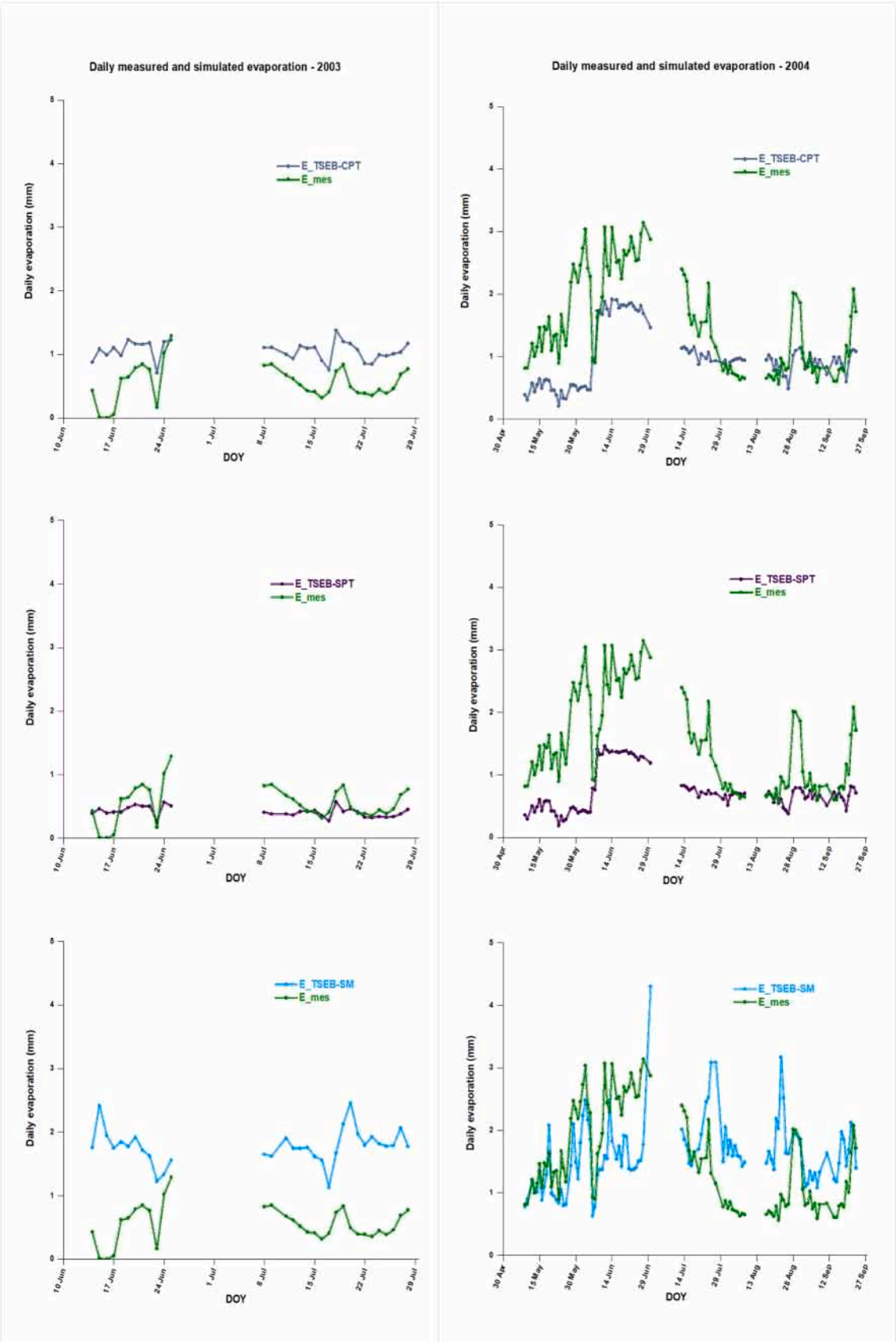

Fig. 10. plot of estimated and simulated evaporation by TSEB-CPT, TSEB-SPT and TSEB-SM, at daily timescale, during the summer period of 2003 (left) and 2004 (right).

dates the corresponding SM levels were low, which increases the ET contribution from the soil surface. Therefore, the formula used to compute E should be revisited. This is particularly relevant when the canopy fraction is greater than 0.5, making it impossible to calibrate arss and brss coefficients for soil surface resistance calculations. The formulation suggested by Song et al. (2016) or the one proposed by Merlin et al. (2016) can be used for E component calculation. Alternatively, the implementation of the soil module improved by Amazirh et al. (2021) into TSEB-SM model provide promising avenues for these revisions.

Future work may focus on incorporating the stomatal conductance into the TSEB model, and assessing its performance over arboricultural crops under various soil moisture regimes. In fact, Gan and Gao (2015) introduced this approach through the replacement of the Priestley-Taylor assumption with a biophysical canopy conductance model in the TSEB model, and adjustment of the under-canopy resistance's formulation. The findings are encouraging, demonstrating that the stomatal conductance may serve as a crucial indicator for monitoring crop water status.

Declaration of Competing Interest

The authors declare that they have no known competing financial interests or personal relationships that could have appeared to influence the work reported in this paper.

Data Availability

Data will be made available on request.

Acknowledgments

The present work is financially supported by ASSIWAT project funded by the OCP Group S.A (Office Chérifien des Phosphates) (grant agreement no: AS_71). We thank the Tensift Observatory in the frame of the SudMed project and the TREMA International Joint Laboratory (https://www.lmi-trema.ma/) for the experimental set-up and providing us with the data of the study site. We would like to thank also the Moroccan Ministry of Higher Education, Scientific Research and Innovation and the OCP Foundation who funded this work through the APRD research program (GEANTech). In addition, we acknowledge the support provided by PRIMA-IDEWA and PRIMA BIOMEnext projects. Finally, we extend our sincere appreciation to the three anonymous reviewers for their comments and constructive suggestions to enhance the quality of our work.

Appendix A

For an analysis purpose, Fig. 11 also displays the time series of daily VPD and of normalized SM at 5 cm and 40 cm depth, throughout the same period. For visualization purpose, soil moisture at field capacity and at wilting point, as well as soil moisture measured at 5 cm depth (top) and 40 cm depth (root zone), are normalized by saturation (θ_{sat}) and residual (θ_r) soil moistures, where the latter are estimated using empirical equations that account for soil texture. To normalize the soil moisture at a given depth, for instance the root zone SM ($\theta_{40\ cm}$), the latter is subtracted from the residual moisture value and the result is divided by the difference between the saturation and the residual moisture values (($\theta_{40\ cm}$- θ_r) / (θ_{sat}- θ_r)).

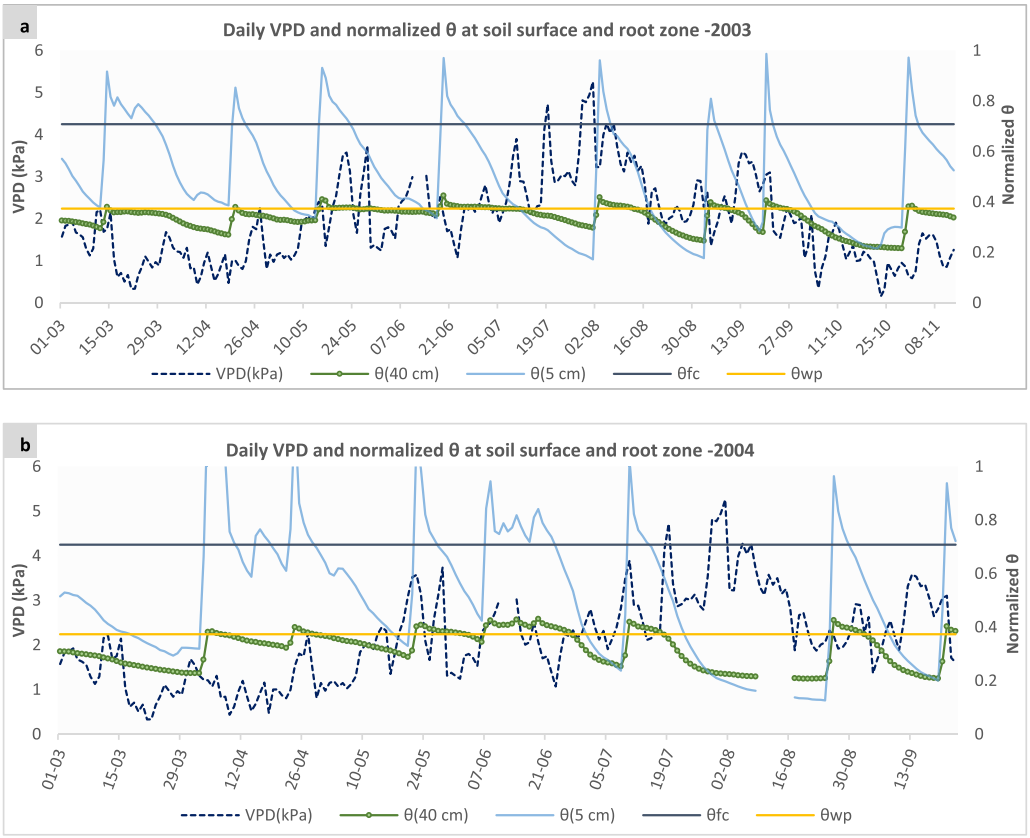

Fig. 11. Daily variation of VPD and normalized soil moisture at top-5 cm and 40 cm (root zone) in Agdal orchard during 2003 (a) and 2004 (b).

Appendix B. The following table outlines all the annotations and abbreviations utilized in the present manuscript

Index of Notations and Abbreviations	
E	Evaporation
EC	Eddy-Covariance
Eeq	Equilibrium evaporation
ET	Actual evapotranspiration
ETc	Crop evapotranspiration
fc	Vegetation fraction cover
G	Soil heat flux
H	Sensible heat flux
HPM	Heat- Pulse-Method
HRM	Heat-Ratio-Method
LAI	Leaf Area Index
LE	Latent heat flux
LST	Land Surface Temperature
NDVI	Normalized Difference Vegetation Index
NIR	Near Infrared channel
PM	Penman-Monteith
αPT	Priestley-Taylor coefficient
R	Red channel
rah	Aerodynamic resistance to heat transport
Rn	Net radiation
Rnc	Canopy net radiation
Rns	Soil net radiation
rs	Resistance to heat flux in the boundary layer immediately above the soil surface
rss	Soil surface resistance
SEB	Surface-Energy-Balance
SM	Soil moisture
T	Transpiration
Tc	Canopy temperature
TDR	Time Domain Reflectometry
TIR	Thermal Infrared Radiance
Trad	Radiometric surface temperature
Ts	Soil temperature
TSEB	Two-Source-Energy-Balance
TSEB-CPT	Two-Source-Energy-Balance-Computed-Priestley-Taylor
TSEB-SM	Two-Source-Energy-Balance-Soil-Moisture
TSEB-SPT	Two-Source-Energy-Balance-Standard-Priestley-Taylor
VPD	Vapor Pressure Deficit

References

Abioye, E.A., Abidin, M.S.Z., Mahmud, M.S.A., Buyamin, S., Ishak, M.H.I., Rahman, M.K. I.A., Otuoze, A.O., Onotu, P., Ramli, M.S.A., 2020. A review on monitoring and advanced control strategies for precision irrigation. Comput. Electron. Agric. 173, 105441 https://doi.org/10.1016/j.compag.2020.105441.

Acharya, B., Sharma, V., 2021. Comparison of satellite driven surface energy balance models in estimating crop evapotranspiration in semi-arid to arid inter-mountain region. Remote Sens. https://doi.org/10.3390/rs13091822.

Agam, N., Kustas, W.P., Anderson, M.C., Norman, J.M., Colaizzi, P.D., Howell, T.A., Prueger, J.H., Meyers, T.P., Wilson, T.B., 2010. Application of the priestley-taylor approach in a two-source surface energy balance model. J. Hydrometeorol. 11, 185–198. https://doi.org/10.1175/2009JHM1124.1.

Aguirre-García, S.D., Aranda-Barranco, S., Nieto, H., Serrano-Ortiz, P., Sánchez-Cañete, E.P., Guerrero-Rascado, J.L., 2021. Modelling actual evapotranspiration using a two source energy balance model with Sentinel imagery in herbaceous-free and herbaceous-cover Mediterranean olive orchards. Agric. . Meteor. 311. https://doi.org/10.1016/j.agrformet.2021.108692.

Ai, Z., Yang, Y., 2016. Modification and validation of Priestley-Taylor model for estimating cotton evapotranspiration under plastic mulch condition. J. Hydrometeorol. 17, 1281–1293. https://doi.org/10.1175/JHM-D-15-0151.1.

Ait Hssaine, B., Merlin, O., Ezzahar, J., Ojha, N., Er-Raki, S., Khabba, S., 2020. An evapotranspiration model self-calibrated from remotely sensed surface soil moisture, land surface temperature and vegetation cover fraction: application to disaggregated SMOS and MODIS data. Hydrol. Earth Syst. Sci. 24, 1781–1803. https://doi.org/10.5194/hess-24-1781-2020.

Ait Hssaine, B.A., Merlin, O., Rafi, Z., Ezzahar, J., Jarlan, L., Khabba, S., Er-Raki, S., 2018. Calibrating an evapotranspiration model using radiometric surface temperature, vegetation cover fraction and near-surface soil moisture data. Agric. . Meteorol. 256–257, 104–115. https://doi.org/10.1016/j.agrformet.2018.02.033.

Ait Hssaine, B.A., Chehbouni, A., Er-Raki, S., Khabba, S., Ezzahar, J., Ouaadi, N., Ojha, N., Rivalland, V., Merlin, O., 2021. On the utility of high-resolution soil moisture data for better constraining thermal-based energy balance over three semi-arid agricultural areas. Remote Sens 13, 1–23. https://doi.org/10.3390/rs13040727.

Allen, R.G., Pereira, L.S., Raes, D., Smith, M., 1998. Crop evapotranspiration-Guidel. Comput. Crop Water Requir. -FAO Irrig. Drain. Pap. 56.

Allen, R.G., Pereira, L.S., Howell, T.A., Jensen, M.E., 2011. Evapotranspiration information reporting: II. Recommended documentation. Agric. Water Manag. 98, 921–929. https://doi.org/10.1016/j.agwat.2010.12.016.

Amazirh, A., Er-Raki, S., Chehbouni, A., Rivalland, V., Diarra, A., Khabba, S., Ezzahar, J., Merlin, O., 2017. Modified Penman–Monteith equation for monitoring evapotranspiration of wheat crop: relationship between the surface resistance and remotely sensed stress index. Biosyst. Eng. 164, 68–84. https://doi.org/10.1016/j.biosystemseng.2017.09.015.

Amazirh, A., Merlin, O., Er-Raki, S., Bouras, E.H., Chehbouni, A., 2021. Implementing a new texture-based soil evaporation reduction coefficient in the FAO dual crop coefficient method. Agric. Water Manag. 250, 106827 https://doi.org/10.1016/j.agwat.2021.106827.

Anderson, M.C., 2012. Mapping daily evapotranspiration at Landsat spatial scales during the BEAREX ' 08 field campaign.

Andreu, A., Kustas, W.P., Polo, M.J., Carrara, A., Gonz, M.P., 2018. Modeling surface energy fluxes over a dehesa (Oak Savanna) ecosystem using a thermal based two-source energy balance model (TSEB) I. Remote Sens 1–27 doi:10.339.

AQUASTAT, 2014. FAO's Global Information System on Water and Agriculture. Rome, Food and Agriculture Organization of the United Nations (FAO). www.fao.org/aquastat/en/.

Baldocchi, D.D., Xu, L., 2007. What limits evaporation from Mediterranean oak woodlands - the supply of moisture in the soil, physiological control by plants or the demand by the atmosphere? Adv. Water Resour. 30, 2113–2122. https://doi.org/10.1016/j.advwatres.2006.06.013.

Baldocchi, D.D., Xu, L., Kiang, N., 2004. How plant functional-type, weather, seasonal drought, and soil physical properties alter water and energy fluxes of an oak – grass savanna and an annual grassland, 123, 13–39. https://doi.org/10.1016/j.agrformet.2003.11.006.

Bashir, M.A., Hata, T., Tanakamaru, H., Abdelhadi, A.W., Tada, A., 2008. Satellite-based energy balance model to estimate seasonal evapotranspiration for irrigated sorghum: a case study from the Gezira scheme, Sudan. Hydrol. Earth Syst. Sci. 12, 1129–1139. https://doi.org/10.5194/hess-12-1129-2008.

Bastiaanssen, W., Meneti, M., Feddes, R.A., Holtslag, a a M., 1998. A remote sensing surface energy balance algorithm for land (SEBAL). J. Hydrol. 212–213, 198–212.

Bellvert, J., Jofre-Čekalović, C., Pelechá, A., Mata, M., Nieto, H., 2020. Feasibility of using the two-source energy balance model (TSEB) with Sentinel-2 and Sentinel-3

images to analyze the spatio-temporal variability of vine water status in a vineyard. Remote Sens 12. https://doi.org/10.3390/rs12142299.
Bouhafa, K., 2022. Management of Olive Tree Fertilization in Morocco. In: Yonar, T. (Ed.), Olive Cultivation. IntechOpen, Rijeka. https://doi.org/10.5772/intechopen.104644.
Boulet, G., Mougenot, B., Lhomme, J., Fanise, P., Olioso, A., Bahir, M., Rivalland, V., 2015. The SPARSE model for the prediction of water stress and evapotranspiration components from thermal infra-red data and its evaluation over irrigated and rainfed wheat 4653–4672. https://doi.org/10.5194/hess-19-4653-2015.
Burchard-Levine, V., Nieto, H., Riaño, D., Migliavacca, M., El-Madany, T.S., Perez-Priego, O., Carrara, A., Martín, M.P., 2020. Seasonal adaptation of the thermal-based two-source energy balance model for estimating evapotranspiration in a semiarid tree-grass ecosystem. Remote Sens 12. https://doi.org/10.3390/rs12060904.
Burgess, S.S.O., Adams, M.A., Turner, N.C., Beverly, C.R., Ong, C.K., Khan, A.A.H., Bleby, T.M., 2001. An improved heat pulse method to measure low and reverse rates of sap flow in woody plants. Tree Physiol. 21, 1157.
Cammalleri, C., Anderson, M.C., Ciraolo, G., Durso, G., Kustas, W.P., La Loggia, G., Minacapilli, M., 2010. The impact of in-canopy wind profile formulations on heat flux estimation in an open orchard using the remote sensing-based two-source model. Hydrol. Earth Syst. Sci. 14, 2643–2659. https://doi.org/10.5194/hess-14-2643-2010.
Cammalleri, C., Ciraolo, G., Minacapilli, M., Rallo, G., 2013a. Evapotranspiration from an olive orchard using remote sensing-based dual crop coefficient approach. Water Resour. Manag. 27, 4877–4895. https://doi.org/10.1007/s11269-013-0444-7.
Cammalleri, C., Rallo, G., Agnese, C., Ciraolo, G., Minacapilli, M., Provenzano, G., 2013b. Combined use of eddy covariance and sap flow techniques for partition of et fluxes and water stress assessment in an irrigated olive orchard. Agric. Water Manag. 120, 89–97. https://doi.org/10.1016/j.agwat.2012.10.003.
Campbell, G.S., Norman, J.M., 1998. An Introduction to En- vironmental biophysics. springer-Verlag. J. Environ. Qual. https://doi.org/10.2134/jeq1977.00472425000600040036x.
Carr, M.K.V., 2013. The water relations and irrigation requirements of olive (Olea europaea L.): A review. Exp. Agric. 49, 597–639. https://doi.org/10.1017/S0014479713000276.
Chirouze, J., Boulet, G., Jarlan, L., Fieuzal, R., Rodriguez, J.C., Ezzahar, J., Er-Raki, S., Bigeard, G., Merlin, O., Garatuza-Payan, J., Watts, C., Chehbouni, G., 2014. Intercomparison of four remote-sensing-based energy balance methods to retrieve surface evapotranspiration and water stress of irrigated fields in semi-arid climate. Hydrol. Earth Syst. Sci. 18, 1165–1188. https://doi.org/10.5194/hess-18-1165-2014.
Choudhury, B.J., 1987. Relationships between vegetation indices, radiation absorption, and net photosynthesis evaluated by a sensitivity analysis. Remote Sens. Environ. 22, 209–233. https://doi.org/10.1016/0034-4257(87)90059-9.
Colaizzi, P.D., Agam, N., Tolk, J.A., Evett, S.R., Howell, T.A., Gowda, P.H., O'Shaughnessy, S.A., Kustas, W.P., Anderson, M.C., 2014. Two-source energy balance model to calculate E, T, and ET: Comparison of priestley-taylor and penman-monteith formulations and two time scaling methods. Trans. ASABE 57, 479–498. https://doi.org/10.13031/trans.57.10423.
Colaizzi, P.D., Agam, N., Tolk, J.A., Evett, S.R., Howell, T.A., O'Shaughnessy, S.A., Gowda, P.H., Kustas, W.P., Anderson, M.C., 2016. Advances in a two-source energy balance model: Partitioning of evaporation and transpiration for cotton. Trans. ASABE 59, 181–197. https://doi.org/10.13031/trans.59.11215.
Davies, J.A., Allen, C.D., 1973. Equilibrium, Potential and Actual Evaporation from Cropped Surfaces in Southern Ontario. J. Appl. Meteorol. Climatol. 12, 649–657.
Diarra, A., Jarlan, L., Er-Raki, S., Le Page, M., Aouade, G., Tavernier, A., Boulet, G., Ezzahar, J., Merlin, O., Khabba, S., 2017. Performance of the two-source energy budget (TSEB) model for the monitoring of evapotranspiration over irrigated annual crops in North Africa. Agric. Water Manag. 193, 71–88. https://doi.org/10.1016/j.agwat.2017.08.007.
Duchemin, B., Hadria, R., Erraki, S., Boulet, G., Maisongrande, P., Chehbouni, A., Escadafal, R., Ezzahar, J., Hoedjes, J.C.B., Kharrou, M.H., Khabba, S., Mougenot, B., Olioso, A., Rodriguez, J.C., Simonneaux, V., 2006. Monitoring wheat phenology and irrigation in Central Morocco: On the use of relationships between evapotranspiration, crops coefficients, leaf area index and remotely-sensed vegetation indices. Agric. Water Manag. 79, 1–27. https://doi.org/10.1016/j.agwat.2005.02.013.
Elfarkh, J., Ezzahar, J., Er-Raki, S., Simonneaux, V., Hssaine, B.A., Rachidi, S., Brut, A., Rivalland, V., Khabba, S., Chehbouni, A., Jarlan, L., 2020. Multi-scale evaluation of the TSEB model over a complex agricultural landscape in Morocco. Remote Sens 12. https://doi.org/10.3390/rs12071181.
Elfarkh, J., Simonneaux, V., Jarlan, L., Ezzahar, J., Boulet, G., Chakir, A., Er-Raki, S., 2022. Evapotranspiration estimates in a traditional irrigated area in semi-arid Mediterranean. Comparison of four remote sensing-based models. Agric. Water Manag. 270, 107728 https://doi.org/10.1016/j.agwat.2022.107728.
Er-Raki, S., Chehbouni, A., Guemouria, N., Duchemin, B., Ezzahar, J., Hadria, R., 2007. Combining FAO-56 model and ground-based remote sensing to estimate water consumptions of wheat crops in a semi-arid region. Agric. Water Manag. 87, 41–54. https://doi.org/10.1016/j.agwat.2006.02.004.
Er-Raki, S., Chehbouni, A., Hoedjes, J., Ezzahar, J., Duchemin, B., Jacob, F., 2008. Improvement of FAO-56 method for olive orchards through sequential assimilation of thermal infrared-based estimates of ET. Agric. Water Manag. 95, 309–321. https://doi.org/10.1016/j.agwat.2007.10.013.
Er-Raki, S., Chehbouni, A., Guemouria, N., Ezzahar, J., Khabba, S., Boulet, G., Hanich, L., 2009. Citrus orchard evapotranspiration: Comparison between eddy covariance measurements and the FAO-56 approach estimates. Plant Biosyst. 143, 201–208. https://doi.org/10.1080/11263500802709897.
Er-Raki, S., Chehbouni, A., Boulet, G., Williams, D.G., 2010. Using the dual approach of FAO-56 for partitioning ET into soil and plant components for olive orchards in a semi-arid region. Agric. Water Manag. 97, 1769–1778. https://doi.org/10.1016/j.agwat.2010.06.009.
Ezzahar, J., Chehbouni, A., Hoedjes, J.C.B., Er-Raki, S., Chehbouni, Ah, Boulet, G., Bonnefond, J.M., De Bruin, H.A.R., 2007. The use of the scintillation technique for monitoring seasonal water consumption of olive orchards in a semi-arid region. Agric. Water Manag. 89, 173–184. https://doi.org/10.1016/j.agwat.2006.12.015.
FAOSTAT, 2023. http://www.fao.org/faostat/en/#data/QC. Site accessed in 2023.
Feng, J., Wang, W., Che, T., Xu, F., 2023. Performance of the improved two-source energy balance model for estimating evapotranspiration over the heterogeneous surface. Agric. Water Manag. 278, 108159 https://doi.org/10.1016/j.agwat.2023.108159.
Fernández, J.E., Cuevas, M.V., Perez-Martin, A., Rodriguez-Dominguez, C.M., Hernandez-Santana, V., Romero, R., García, J.M., Montero, A., Padilla-Díaz, C.M., Egea, G., Alcon, F., Ruiz, M.P., García-Tejero, I.F., Diaz-Espejo, A., 2018. New approaches for precise irrigation in hedgerow olive orchards. Acta Hortic. (1199), 225–239. https://doi.org/10.17660/ActaHortic.2018.1199.36.
Fernández, J.E., Moreno, F., Girón, I.F., Blázquez, O.M., 1997. Stomatal control of water use in olive tree leaves. Plant Soil 190, 179–192. https://doi.org/10.1023/A:1004293026973.
Fernández, J.E., Palomo, M.J., Clothier, B.E., Ferna, J.E., Moreno, F., Green, S.R., Giro, I. F., 2001. Heat-pulse measurements of sap ow in olives for automating irrigation: tests, root ow and diagnostics of water stress. Agric. Water Manag. 51, 99–123.
Flint, A.L., Childs, S.W., 1991. Use of the Priestley-Taylor evaporation equation for soil water limited conditions in a small forest clearcut. Agric. . Meteorol. 56, 247–260. https://doi.org/10.1016/0168-1923(91)90094-7.
French, A.N., 2001. Scaling Surf. Energy Fluxes Using Remote. Sense Data 362.
Fuentes-Peñailillo, F., Ortega-Farías, S., Acevedo-Opazo, C., Fonseca-Luengo, D., 2018. Implementation of a two-source model for estimating the spatial variability of olive evapotranspiration using satellite images and ground-based climate data. Water (Switz.) 10. https://doi.org/10.3390/w10030339.
Gan, G., Gao, Y., 2015. Estimating time series of land surface energy fluxes using optimized two source energy balance schemes: Model formulation, calibration, and validation. Agric. . Meteorol. 208, 62–75. https://doi.org/10.1016/j.agrformet.2015.04.007.
Gan, G., Kang, T., Yang, S., Bu, J., Feng, Z., Gao, Y., 2019. An optimized two source energy balance model based on complementary concept and canopy conductance. Remote Sens. Environ. 223, 243–256. https://doi.org/10.1016/j.rse.2019.01.020.
Gao, R., Torres-Rua, A.F., Nieto, H., Zahn, E., Hipps, L., Kustas, W.P., Alsina, M.M., Bambach, N., Castro, S.J., Prueger, J.H., Alfieri, J., McKee, L.G., White, W.A., Gao, F., McElrone, A.J., Anderson, M., Knipper, K., Coopmans, C., Gowing, I., Agam, N., Sanchez, L., Dokoozlian, N., 2023. ET Partitioning Assessment Using the TSEB Model and sUAS Information across California Central Valley Vineyards. Remote Sens 15. https://doi.org/10.3390/rs15030756.
Gómez-Candón, D., Bellvert, J., Royo, C., 2021. Performance of the Two-Source Energy Balance (TSEB) Model as a Tool for Monitoring the Response of Durum Wheat to Drought by High-Throughput Field Phenotyping. Front. Plant Sci. 12 https://doi.org/10.3389/fpls.2021.658357.
Granier, A., 1987. Evaluation of transpiration in a Douglas-fir stand by means of sap flow measurements. Tree Physiol. 3, 309–320. https://doi.org/10.1093/treephys/3.4.309.
Gutman, G., Ignatov, A., 1998. The derivation of the green vegetation fraction from NOAA/AVHRR data for use in numerical weather prediction models. Int. J. Remote Sens. 19, 1533–1543. https://doi.org/10.1080/014311698215333.
Guzinski, R., Anderson, M., Nieto, H., Sandholt, I., 2013. Using a thermal-based two source energy balance model with time-differencing to estimate surface energy fluxes with day–night MODIS observations. https://doi.org/10.5194/hess-17-2809-2013.
Häusler, M., Conceição, N., Tezza, L., Sánchez, J.M., Campagnolo, M.L., Häusler, A.J., Silva, J.M.N., Warneke, T., Heygster, G., Ferreira, M.I., 2018. Estimation and partitioning of actual daily evapotranspiration at an intensive olive grove using the STSEB model based on remote sensing. Agric. Water Manag. 201, 188–198. https://doi.org/10.1016/j.agwat.2018.01.027.
Hoedjes, J.C.B., Chehbouni, A., Ezzahar, J., Escadafal, R., De Bruin, H.A.R., 2007. Comparison of large aperture scintillometer and eddy covariance measurements: Can thermal infrared data be used to capture footprint-induced differences? J. Hydrometeorol. 8, 144–159. https://doi.org/10.1175/JHM561.1.
Hoedjes, J.C.B., Chehbouni, A., Jacob, F., Ezzahar, J., Boulet, G., 2008. Deriving daily evapotranspiration from remotely sensed instantaneous evaporative fraction over olive orchard in semi-arid Morocco. J. Hydrol. 354, 53–64. https://doi.org/10.1016/j.jhydrol.2008.02.016.
Horst, T.W., Weil, J.C., 1992. Footprint estimation for scalar flux measurements in the atmospheric surface layer. Bound. -Layer. Meteor. 59, 279–296. https://doi.org/10.1007/BF00119817.
Horst, T.W., Weil, J.C., 1994. How Far is Far Enough?: The Fetch Requirements for Micrometeorological Measurement of Surface Fluxes. Atmos. Ocean. Technol. 11, 1018–1025.
INRA Magazine, 2016. Moroccan National Institute for Agronomic Research of Meknes, Morocco. https://mag.inrameknes.info/?p=1203.
Jury, W.A., Tanner, C.B., 1975. Advection Modification of the Priestley and Taylor Evapotranspiration Formula. Agron. J. 67, 840–842.
Kalma, J.D., McVicar, T.R., McCabe, M.F., 2008. Estimating land surface evaporation: A review of methods using remotely sensed surface temperature data. Surv. Geophys. 29, 421–469. https://doi.org/10.1007/s10712-008-9037-z.

Kanemasu, E.T., Stone, L.R., Powers, W.L., 1976. Evapotranspiration Model Tested for Soybean and Sorghum. Agron. J. 68, 569–572. https://doi.org/10.2134/agronj1976.00021962006800040009x.

Kassout, J., Ater, M., Ivorra, S., Barbara, H., Limier, B., Ros, J., Girard, V., Paradis, L., Terral, J.F., 2021. Resisting aridification: adaptation of sap conduction performance in moroccan wild olive subspecies distributed over an aridity gradient. Front. Plant Sci. 12, 1–14. https://doi.org/10.3389/fpls.2021.663721.

Kato, T., Kimura, R., Kamichika, M., 2004. Estimation of evapotranspiration, transpiration ratio and water-use efficiency from a sparse canopy using a compartment model. Agric. Water Manag. 65, 173–191. https://doi.org/10.1016/j.agwat.2003.10.001.

Kharrou, M.H., Le Page, M., Chehbouni, A., Simonneaux, V., Er-Raki, S., Jarlan, L., Ouzine, L., Khabba, S., Chehbouni, G., 2013. Assessment of Equity and Adequacy of Water Delivery in Irrigation Systems Using Remote Sensing-Based Indicators in Semi-Arid Region, Morocco. Water Resour. Manag. 27, 4697–4714. https://doi.org/10.1007/s11269-013-0438-5.

Khriji, S., El Houssaini, D., Jmal, M.W., Viehweger, C., Abid, M., Kanoun, O., 2014. Precision irrigation based on wireless sensor network. IET Sci. Meas. Technol. 8, 98–106. https://doi.org/10.1049/iet-smt.2013.0137.

Kustas, W., Norman, J., Schmugge, T., 2004. Mapping surface energy fluxes with radiometric temperature. https://doi.org/10.1201/9780203502174-c8.

Kustas, W.P., Norman, J.M., 1999. Evaluation of soil and vegetation heat flux predictions using a simple two-source model with radiometric temperatures for partial canopy cover. Agric. . Meteorol. 94, 13–29. https://doi.org/10.1016/S0168-1923(99)00005-2.

Kustas, W.P., Nieto, H., Morillas, L., Anderson, M.C., Alfieri, J.G., Hipps, L.E., Villagarcía, L., Domingo, F., Garcia, M., 2016. Revisiting the paper "Using radiometric surface temperature for surface energy flux estimation in Mediterranean drylands from a two-source perspective. Remote Sens. Environ. 184, 645–653. https://doi.org/10.1016/j.rse.2016.07.024.

Kustas, W.P., Alfieri, J.G., Nieto, H., Wilson, T.G., Gao, F., Anderson, M.C., 2019. Utility of the two-source energy balance (TSEB) model in vine and interrow flux partitioning over the growing season. Irrig. Sci. 37, 375–388. https://doi.org/10.1007/s00271-018-0586-8.

Li, M., Zhou, J., Peng, Z., Liu, S., Göttsche, F., 2019. Agricultural and Forest Meteorology Component radiative temperatures over sparsely vegetated surfaces and their potential for upscaling land surface temperature. Agric. . Meteorol. 276–277, 107600 https://doi.org/10.1016/j.agrformet.2019.05.031.

López-Olivari, R., Ortega-Farías, S., Poblete-Echeverría, C., 2016. Partitioning of net radiation and evapotranspiration over a superintensive drip-irrigated olive orchard. Irrig. Sci. 34, 17–31. https://doi.org/10.1007/s00271-015-0484-2.

Luo, Y., Id, T.S.E., Filippa, G., Id, X.M., Id, B.A., Carrara, A., Gonzalez-cascon, R., Cremonese, E., Id, G.M., Perez-priego, O., Reichstein, M., Richardson, A.D., 2018. Using Near-Infrared-Enabled Digital Repeat Photography to Track Structural and Physiological Phenology in Mediterranean Tree – Grass Ecosystems. https://doi.org/10.3390/rs10081293.

Massman, W., 1987. A comparative study of some mathematical mod- els of the mean wind structure and aerodynamic drag of plant canopies. Bound. -Layer. Meteor. 40, 179–197.

Merlin, O., Chirouze, J., Olioso, A., Jarlan, L., Chehbouni, G., Boulet, G., 2014. An image-based four-source surface energy balance model to estimate crop evapotranspiration from solar reflectance/thermal emission data (SEB-4S). Agric. . Meteorol. 184, 188–203. https://doi.org/10.1016/j.agrformet.2013.10.002.

Merlin, O., Stefan, V.G., Amazirh, A., Chanzy, A., Ceschia, E., Er-Raki, S., Gentine, P., Tallec, T., Ezzahar, J., Bircher, S., Beringer, J., Khabba, S., 2016. Modeling soil evaporation efficiency in a range of soil and atmospheric conditions using a meta-analysis approach. Water Resour. Res. 52, 3663–3684. https://doi.org/10.1002/2015WR018233.

Morillas, L., García, M., Nieto, H., Villagarcia, L., Sandholt, I., Gonzalez-dugo, M.P., 2013. Using radiometric surface temperature for surface energy fl ux estimation in Mediterranean drylands from a two-source perspective. Remote Sens. Environ. 136, 234–246. https://doi.org/10.1016/j.rse.2013.05.010.

Nieto, H., Alsina, M.M., Kustas, W.P., García-Tejera, O., Chen, F., Bambach, N., Gao, F., Alfieri, J.G., Hipps, L.E., Prueger, J.H., McKee, L.G., Zahn, E., Bou-Zeid, E., McElrone, A.J., Castro, S.J., Dokoozlian, N., 2022. Evaluating different metrics from the thermal-based two-source energy balance model for monitoring grapevine water stress. Irrig. Sci. 40, 697–713. https://doi.org/10.1007/s00271-022-00790-2.

Norman, J.M., Kustas, W.P., Humes, K.S., 1995. Source approach for estimating soil and vegetation energy fluxes in observations of directional radiometric surface temperature. Agric. . Meteorol. 77, 263–293. https://doi.org/10.1016/0168-1923(95)02265-Y.

Ortega-Farías, S., López-Olivari, R., 2012. Validation of a two-layer model to estimate latent heat flux and evapotranspiration in a drip-irrigated olive orchard. Trans. ASABE 55, 1169–1178.

Ortega-Farías, S., Ortega-Salazar, S., Poblete, T., Kilic, A., Allen, R., Poblete-Echeverría, C., Ahumada-Orellana, L., Zuñiga, M., Sepúlveda, D., 2016. Estimation of energy balance components over a drip-irrigated olive orchard using thermal and multispectral cameras placed on a helicopter-based unmanned aerial vehicle (UAV). Remote Sens 8, 1–18. https://doi.org/10.3390/rs8080638.

Passerat de Silans, A., Vauclin, M., Bois, P., Saugier, B., Guennelon, R., Vachaud, G., (Grenoble)., I. national polytechnique, (1966-1991)., I. de mécanique de G., 1986. Transferts de masse et de chaleur dans un sol stratifié soumis à une excitation atmosphérique naturelle: comparaison: modèles-expérience. TA - TT -. https://doi.org/LK - https://worldcat.org/title/490217472.

Penman, H.L., 1948. Natural evaporation from open water, bare soil and grass. Proc. R. Soc. Lond. A. Math. Phys. Sci. 193, 120–145.

Pereira, L.S., Allen, R.G., Smith, M., Raes, D., 2015. Crop evapotranspiration estimation with FAO56: Past and future. Agric. Water Manag. 147, 4–20. https://doi.org/10.1016/j.agwat.2014.07.031.

Priestley, C.H.B., Taylor, R.J., 1972. On the Assessment of Surface Heat Flux and Evaporation Using Large-Scale Parameters. Mon. Weather Rev. 100, 81–92. https://doi.org/10.1175/1520-0493(1972)100<0081:otaosh>2.3.co;2.

Puig-sirera, A., Rallo, G., Paredes, P., Paço, T.A., Minacapilli, M., Provenzano, G., Pereira, L.S., 2021. Transpiration and Water Use of an Irrigated Traditional Olive Coefficient Approach. Water 13, 2466.

Rafi, Z., Merlin, O., Le Dantec, V., Khabba, S., Mordelet, P., Er-Raki, S., Amazirh, A., Olivera-Guerra, L., Ait Hssaine, B., Simonneaux, V., Ezzahar, J., Ferrer, F., 2019. Partitioning evapotranspiration of a drip-irrigated wheat crop: Inter-comparing eddy covariance-, sap flow-, lysimeter- and FAO-based methods. Agric. . Meteorol. 265, 310–326. https://doi.org/10.1016/j.agrformet.2018.11.031.

Raupach, M.R., 2000. Equilibrium evaporation and the convective boundary layer. Bound. -Layer. Meteor. 96, 107–142. https://doi.org/10.1023/a:1002675729075.

Rozenstein, O., Fine, L., Malachy, N., Richard, A., Pradalier, C., Tanny, J., 2023. Data-driven estimation of actual evapotranspiration to support irrigation management: Testing two novel methods based on an unoccupied aerial vehicle and an artificial neural network. Agric. Water Manag. 283, 108317 https://doi.org/10.1016/j.agwat.2023.108317.

Saadi, S., Boulet, G., Bahir, M., Brut, A., Delogu, É., Fanise, P., Mougenot, B., Simonneaux, V., Chabaane, Z.L., 2018. Assessment of actual evapotranspiration over a semiarid heterogeneous land surface by means of coupled low-resolution remote sensing data with an energy balance model: Comparison to extra-large aperture scintillometer measurements. Hydrol. Earth Syst. Sci. 22, 2187–2209. https://doi.org/10.5194/hess-22-2187-2018.

Santanello, J.A., Friedl, M.A., 2003. Diurnal covariation in soil heat flux and net radiation. J. Appl. Meteor. 42, 851–862. https://doi.org/10.1175/1520-0450(2003)042<0851:DCISHF>2.0.CO;2.

Sanz-Cortés, F., Martinez-Calvo, J., Badenes, M.L., Bleiholder, H., Hack, H., Llacer, G., Meier, U., 2002. Phenological growth stages of olive trees (Olea europaea). Ann. Appl. Biol. 140, 151–157. https://doi.org/10.1111/j.1744-7348.2002.tb00167.x.

Sellers, P.J., Heiser, M.D., Hall, F.G., 1992. Relations between surface conductance and spectral vegetation indices at intermediate (100m2 to 15km2) length scales. J. Geophys. Res. 97 https://doi.org/10.1029/92jd01096.

Shuttleworth and Wallace, 1985. Evaporation from sparse crops-an energy combination theory 839–855.

Slatyer, R.O., McIlroy, I.C., 1961. Practical Microclimatology; with Special Reference to the Water Factor in Soil, Plant, Atmosphere Relationships [by] R.O. Slatyer [and] I. C. McIlroy, Practical Microclimatology; with Special Reference to the Water Factor in Soil, Plant, Atmosphere Relationships [by] R.O. Slatyer [and] I.C. McIlroy. UNESCO.

Song, L., Ding, Z., Kustas, W.P., Xu, Y., Zhao, G., Liu, S., Ma, M., Xue, K., Bai, Y., Xu, Z., 2022. Applications of a thermal-based two-source energy balance model coupled to surface soil moisture. Remote Sens. Environ. 271, 112923 https://doi.org/10.1016/j.rse.2022.112923.

Song, L., Kustas, W.P., Liu, S., Colaizzi, P.D., Nieto, H., Xu, Z., Ma, Y., Li, M., Xu, T., Agam, N., Tolk, J.A., Evett, S.R., 2016. Applications of a thermal-based two-source energy balance model using Priestley-Taylor approach for surface temperature partitioning under advective conditions. J. Hydrol. 540, 574–587. https://doi.org/10.1016/j.jhydrol.2016.06.034.

Su, Z., 2002. The Surface Energy Balance System (SEBS) for estimation of turbulent heat fluxes. SEBS - Surf. Energy Balance 6, 85–100.

Tanasijevic, L., Todorovic, M., Pereira, L.S., Pizzigalli, C., Lionello, P., 2014. Impacts of climate change on olive crop evapotranspiration and irrigation requirements in the Mediterranean region. Agric. Water Manag. 144, 54–68. https://doi.org/10.1016/j.agwat.2014.05.019.

Tanner, C.B., Jury, W.A., 1976. Estimating Evaporation and Transpiration from a Row Crop during Incomplete Cover 1. Agron. J. 68, 239–243. https://doi.org/10.2134/agronj1976.00021962006800020007x.

Taylor, K.E., 2001. Summarizing multiple aspects of model performance in a single diagram. J. Geophys. Res. Atmos. 106, 7183–7192.

Timmermans, W.J., Kustas, W.P., Anderson, M.C., French, A.N., 2007. An intercomparison of the Surface Energy Balance Algorithm for Land (SEBAL) and the Two-Source Energy Balance (TSEB) modeling schemes. Remote Sens. Environ. 108, 369–384. https://doi.org/10.1016/j.rse.2006.11.028.

Toumi, J., Er-Raki, S., Ezzahar, J., Khabba, S., Jarlan, L., Chehbouni, A., 2016. Performance assessment of AquaCrop model for estimating evapotranspiration, soil water content and grain yield of winter wheat in Tensift Al Haouz (Morocco): Application to irrigation management. Agric. Water Manag. 163, 219–235. https://doi.org/10.1016/j.agwat.2015.09.007.

Twine, T.E., Kustas, W.P., Norman, J.M., Cook, D.R., Houser, P.R., Meyers, T.P., Prueger, J.H., Starks, P.J., Wesely, M.L., 2000. Correcting eddy-covariance flux underestimates over a grassland. Agric. . Meteorol. 103, 279–300. https://doi.org/10.1016/S0168-1923(00)00123-4.

Wahbi, S., Wakrim, R., Aganchich, B., Tahi, H., Serraj, R., 2005. Effects of partial rootzone drying (PRD) on adult olive tree (Olea europaea) in field conditions under arid climate: I. Physiological and agronomic responses. Agric. Ecosyst. Environ. 106, 289–301. https://doi.org/10.1016/j.agee.2004.10.015.

Williams, D.G., Cable, W., Hultine, K., Hoedjes, J.C.B., Yepez, E.A., Simonneaux, V., Er-Raki, S., Boulet, G., De Bruin, H.A.R., Chehbouni, A., Hartogensis, O.K., Timouk, F., 2004. Evapotranspiration components determined by stable isotope, sap flow and eddy covariance techniques. Agric. . Meteorol. 125, 241–258. https://doi.org/10.1016/j.agrformet.2004.04.008.

Wösten, J.H.M., 1997. Pedotransfer functions to evaluate soil quality. Dev. Soil Sci. 25, 221–245. https://doi.org/10.1016/S0166-2481(97)80037-2.
Wu, H., Zhu, W., Huang, B., 2021. Seasonal variation of evapotranspiration, Priestley-Taylor coefficient and crop coefficient in diverse landscapes. Geogr. Sustain. https://doi.org/10.1016/j.geosus.2021.09.002.
WWAP, 2020. United Nations World Water Development Report 2020: Water and climate change. Unesco.
Yang, Y., Su, H., Zhang, R., Tian, J., Li, L., 2015. An enhanced two-source evapotranspiration model for land (ETEML): Algorithm and evaluation. Remote Sens. Environ. 168, 54–65. https://doi.org/10.1016/j.rse.2015.06.020.
Yimam, Y.T., Ochsner, T.E., Kakani, V.G., 2015. Evapotranspiration partitioning and water use efficiency of switchgrass and biomass sorghum managed for biofuel. Agric. Water Manag. 155, 40–47. https://doi.org/10.1016/j.agwat.2015.03.018.
Zhang, B., Kang, S., Li, F., Zhang, L., 2008. Comparison of three evapotranspiration models to Bowen ratio-energy balance method for a vineyard in an arid desert region of northwest China. Agric. . Meteorol. 148, 1629–1640. https://doi.org/10.1016/j.agrformet.2008.05.016.
Zhou, S., Yu, B., Zhang, Y., Huang, Y., Guangqian, W., 2016. Partitioning evapotranspiration based on the concept of underlying water use efficiency. Water Resour. Res. 1160, 1175. https://doi.org/10.1002/2015WR017766.Received.
Zuñiga, M., Ortega-Farías, S., Poblete-Echeverría, C., 2014. Use of sap flow sensors to determine transpiration of a young drip-irrigated olive orchard ('Arbequina') under semi-arid conditions. Acta Hortic. (1057), 405–410. https://doi.org/10.17660/ActaHortic.2014.1057.50.